Worcester Polytechnic Institute
Digital WPI

Major Qualifying Projects (All Years) | Major Qualifying Projects

April 2015

Wireless Charging of Mobile Systems

Douglas Perez
Worcester Polytechnic Institute

Jacob Dean Cooley
Worcester Polytechnic Institute

Jeremy Tyler Giguere
Worcester Polytechnic Institute

Follow this and additional works at: https://digitalcommons.wpi.edu/mqp-all

Repository Citation
Perez, D., Cooley, J. D., & Giguere, J. T. (2015). *Wireless Charging of Mobile Systems*. Retrieved from https://digitalcommons.wpi.edu/mqp-all/3355

This Unrestricted is brought to you for free and open access by the Major Qualifying Projects at Digital WPI. It has been accepted for inclusion in Major Qualifying Projects (All Years) by an authorized administrator of Digital WPI. For more information, please contact digitalwpi@wpi.edu.

Worcester Polytechnic Institute

Major Qualifying Project

A Major Qualifying Project Submitted to the Faculty of Worcester Polytechnic Institute in Partial Fulfillment of the Requirements for a Degree in Bachelor of Science in Electrical and Computer Engineering

Wireless Charging of Mobile Systems

JAO - 1503

Author:

Jacob Cooley

Jeremy Giguere

Douglas Perez

Submitted To:

Dr. John Orr

April 30, 2015

Abstract

This project designs and implements a wireless charging system for small industrial mobile applications. A quick, efficient charging system allows for maximum resource utilization and minimized "down time." Resonant inductive power transfer is demonstrated for this purpose. The efficiency of such a system is analyzed, and the results are promising, however there are significant opportunities for improvement.

Acknowledgments

This project would have never happened if we had not received substantial assistance from a number of very supportive individuals. We would like to thank our advisor, Professor Orr for his inexhaustible patience and positivity. Thanks to him, we were able to work though every roadblock that this project threw at us. We would also like to thank Robert Brown from the ECE Shop for always making himself available to help in any way he could. We thank Professor Makarov as well, who spent much of his own time teacing us how to utilize ANSYS software necessary for our project. Finally, we would like to thank Malick Kelly providing his own time to help us manufacture important components of our project.

Contents

List of Figures

Chapter 1

Introduction

Many industries, such as medicine, manufacturing, and logistics, could benefit greatly through the use of mobile robots, capable of executing automated and repetitive tasks. These robots would be more efficient and effective than human laborers and would optimize the industries' performance. However, these robots require electrical power to operate. For mobile robots, this can pose a problem. Traditional charging systems require physical contact to transfer power from a source to a battery or other means of electrical energy storage. While this is not an issue for stationary systems, mobile systems need to cease operation in order to charge. Especially for systems that are expected to work continuously, this "down time" necessitates the purchase of additional units to cover for those that are out of service for recharging.

A charging system that can supply power to mobile systems wirelessly, as they work, would reduce or eliminate the need for down time, extra units and wasted resources. This project investigates a wireless charging system based on resonant inductive coupling. To this end, the project first reviews examples of existing work in the field as well as potential options for wireless charging, reaching the conclusion that resonant inductive coupling holds the most potential for an efficient, cost-effective power transfer mechanism. A prototype that demonstrates resonant inductive coupling is built and analyzed, including design and implementation of the power transfer coils and supporting circuitry. Finally, this report draws conclusions and makes recommendations based on the analysis of the prototype.

The goal of this project to design and construct a wireless charging system. Specifically, the goal of this project is to build a wireless charging system for mobile vehicles. The design will have a focus on mobile vehicles that operate close to the ground in a controlled environment, and are expected to operate continuously with minimal downtime—such as a warehouse or factory. The design must be able to charge the vehicles quickly and efficiently, to avoid impacting the vehicle's effectiveness.

Due to the significant complicating factors of designing a mobile robotic system, the scope of this project will be limited to the power transfer system. The system will be designed for a power output on the order of 100 watts.

Chapter 2

Background

The concept of wirelessly powering a device with no need of physical connection has been around for over a century. Nikola Tesla, a late-nineteenth century electrical engineer, pioneered the idea and experimented with transmitting power though the air [1]. Tesla demonstrated this in his laboratory in Colorado Springs, Colorado, where he transmitted power wirelessly at an extremely high voltage and high frequency. Unfortunately for Tesla, wireless power transfer was not particularly practical in his day and age, and his technology did not develop as much as he would have liked. However, the present day proliferation of portable, chargeable electronic devices has jump started the pursuit of wireless power transfer as more and more companies seek to finally "cut the cord" on electric power. This section will discuss various different methods of wireless charging, as well as the market for, and the health and safety aspects of wireless power transmission.

2.1 Wireless Charging Methods

There are a number of methods for transmitting power wirelessly. The most popular and effective of which are inductive coupling, resonant inductive coupling, capacitive coupling, radio frequency and microwave power transmission, and laser power beaming. This section will discuss the different approaches of wireless charging devices.

2.1.1 Inductive Coupling

One of the oldest techniques of transferring energy wirelessly is inductive coupling. An inductor is a wire formed in a coil, where an induced current produces a magnetic field which is based on the principle of electromagnetic induction [2]. Electromagnetic induction was first discovered by English scientist, Michael Faraday in 1831. He found that by moving a magnet through a coil of wire, a voltage was induced across the coil. When a complete path was created, the induced voltage caused an induced current. Faraday's Law states:

- The amount of voltage induced in a coil is directly proportional to the rate of change of the magnetic flux with respect to the coil, $\frac{d\Phi}{dt}$.
- The amount of voltage induced in a coil is directly proportional to the number of turns of wire in the coil (N).

The formula that represents Faraday's Law is the following:

$$V_{ind} = N\frac{d\Phi}{dt} \tag{2.1}$$

Where V_{ind} = the induced voltage
N = number of turns of wire in the coil
$\frac{d\Phi}{dt}$ = the rate of change of the magnetic flux

The induced voltage is proportional to the number of turns of wire in the coil, and to the rate of change of the magnetic field.

Another method of inducing voltage across a coil is to cause the current to fluctuate. When the current changes, the magnetic field also changes. This causes an induced voltage across the coil. The formula below is example of the effects of fluctuating current:

$$V_{ind} = L\frac{di}{dt} \tag{2.2}$$

Where V_{ind} = the induced voltage
L = inductance
$\frac{di}{dt}$ = the rate of change of the current

The induced voltage is directly proportional to the inductance, and to the rate of change of the current. It can be seen from this formula that the faster the current through an inductor changes, the greater the induced voltage will be. In an AC circuit, the induced voltage is directly dependent on frequency. As frequency increases so does the rate of change of the current.

The formula of inductance is as follows:

$$L = \frac{N^2\mu A}{l} \tag{2.3}$$

$$\mu = \mu_r\mu_0 \tag{2.4}$$

Where L = inductance of coil in Henrys
N = Number of turns in wire of coil (straight wire=1)
μ = Permeability of core material($\mu = \mu_r\mu_0$)
μ_r = Relative permeability (1 for air)
μ_0 = Permeability of free space ($4\pi * 10^{-7} H/m$)
A = Area of coil in square meters (πr^2)
l = Average length of coil in meters

Figure 2.1: Simplified circuit illustrating inductive coupling

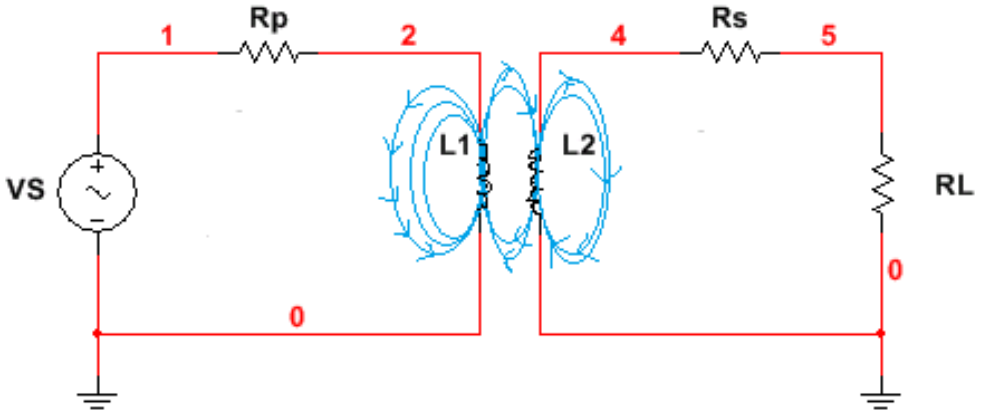

When a second coil is introduced to a changing magnetic field of the primary coil, it will cause an induced voltage in the second coil, thereby magnetically coupling the coils. The voltage induced in the second coil is a function of mutual inductance, calculated by the following formula:

$$L_M = k\sqrt{L_1 L_2} \tag{2.5}$$

Where L_M = Mutual inductance

k = coefficient coupling between the two coils

$$k = \frac{\Phi_2}{\Phi_1}$$

L_1 = Inductance of coil 1

L_2 = Inductance of coil 2

The formulas above describe the principles of induction and how voltage is induced in a second coil. Below is a simplified circuit of inductive coupling:

In the circuit in Figure 2.1, the transmitter has an AC source which is connected a resistor (R_p) and an inductor (L_1), where the resistor represents power loss due to heat. As inductor 1 (L_1) receives the fluctuating current from the AC source it creates a magnetic field and induces voltage in L_2. The receiver circuit which has L_2, R_s, and R_L is powered by the changing magnetic field of the transmitter. Again Rs represents the power loss of the inductor and R_L is the load.

In order to strengthen the magnetic field of an inductor, a ferromagnetic core is inserted between the coils. A ferromagnetic core provides a better path for the magnetic lines of force and increases the amount of coupling between the coils [2].

Devices such as electric toothbrushes, charging mats for cell phones, and medical implants use this method to recharge batteries. Some of the disadvantages of inductive charging are the inefficiency of power transmission at a further distance, inability to control the electromagnetic interference, and the electric heat lost.

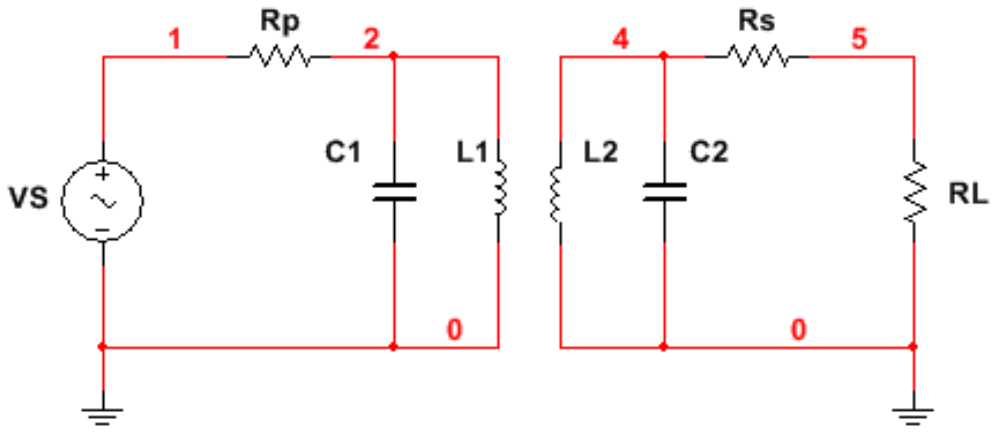

Figure 2.2: Simplified circuit of Resonant Induction Coupling

There have been some attempts ([3],[4]) to reduce transfer loss in inductive coupling. Methods such as implementing ultra-thin coils, higher frequencies, and enhancing drive electronics are possible solutions. When implementing higher frequency induction to deliver high power the efficiency reaches 86%, the other two methods are still being investigated for any improvements.

2.1.2 Resonant Induction

A variation of inductive coupling is Resonant Inductive Coupling (RIC). A RIC circuit adds capacitors to the circuit to tune the circuit to the operating frequency. Resonance is the tendency of a system to oscillate with larger amplitude at some frequencies than at others. Resonance of a circuit involving capacitors and inductors, in parallel, occurs because the collapsing magnetic field of the inductor generates an electric current in its windings that charges the capacitor, and then the discharging capacitor provides an electric current that builds the magnetic field in the inductor. The circuit in Figure 2.2 is a simplified representation of resonant inductive coupling.

In this system, the capacitors in parallel with the inductor set the resonant frequency. The two circuits need to resonate at the same frequency in order for this system to function properly. It is important to note that resonance increases the range of inductive coupling.

In 2007, MIT researchers experimented with self-resonant inductive coils, concluding that resonance enhances power transmission range and strength. The researchers demonstrated this by powering a 60W light bulb at a distance of two meters with an efficiency of 45%. Figure 2.3 is an image showing the 60W light bulb being lit [5].

2.1.3 Capacitive Coupling

A third method for wireless power transfer involves separating the power source and the load with two parallel plates. These plates act as the anode and cathode of a typical parallel plate capacitor. Since the electric field is contained between the plates, there is very little energy leakage. However, this design's effectiveness is heavily dependent upon the available

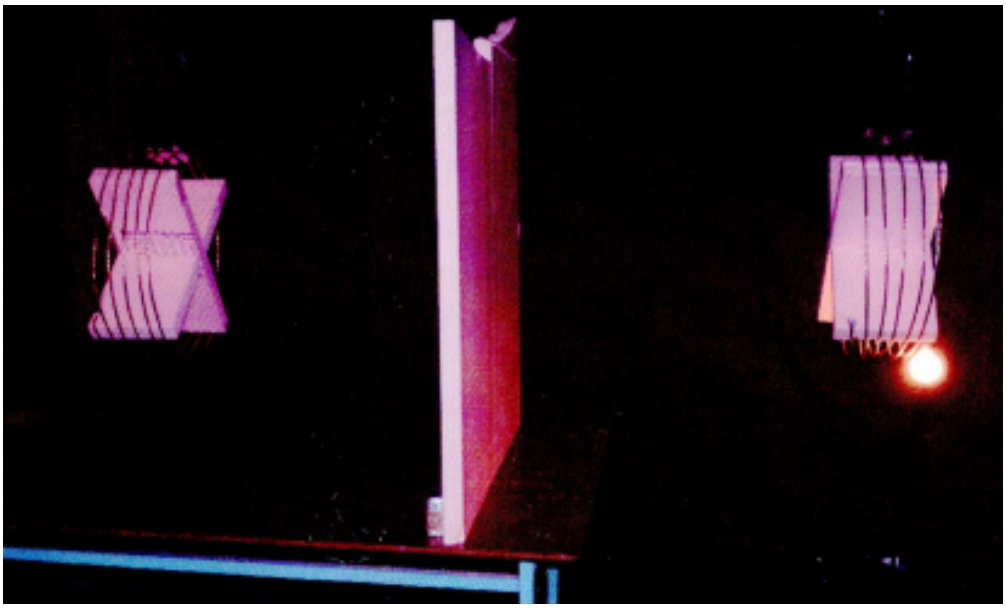

Figure 2.3: MIT lighting 60W bulb 2 meters away

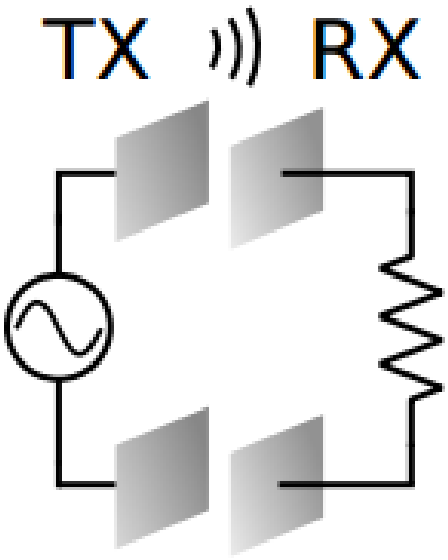

Figure 2.4: Basic capacitive coupled system

area on the receiving system, and the distance between the TX and RX plates. Power is transferred to load based on the relationship:

$$I(t) = C\frac{dV}{dt} \tag{2.6}$$

Where C is the capacitance given by the equation for parallel plate capacitors:

$$C = \frac{\epsilon_r \epsilon_0 A}{d} \tag{2.7}$$

Where $\epsilon_r$is the relative permittivity of air (1 in this case)
A is overlapping area,
d is the separation distance, and
ϵ_0 is the permittivity of a vacuum, $8.854 * 10^{-12} F/m$

Since ϵ_r is approximately 1, the capacitance between the TX and RX plates will be much less than that of equivalently sized parallel plate capacitors. This results in a lower current, and slower energy transfer. This makes it imperative that A be as large as possible and d be as small as possible. However, for mobile systems, particularly small ones, this bears the risk of limiting mobility and consuming valuable space on the platform. On the other hand, however, this method of charging is highly efficient. Most losses come from the source series resistance, R_S. Minimal losses result from the transfer itself. Thus, while the capacitive coupling method may be slower or larger than some alternatives, it is likely the most efficient means of energy transfer [6].

2.1.4 Microwave Power Transmission

Microwaves are widely used for point-to-point communications because their small wavelength allows conveniently-sized antennas to direct them in narrow beams, which can be pointed directly at the receiving antenna. This allows nearby microwave equipment to use the same frequencies without interfering with each other, as lower frequency radio waves do.

Microwave power transfer (MPT) uses the far-field effects of electromagnetic radiation to transfer power wirelessly over long distances. Applications considered include energy transfer from space-based solar stations [7]. The basic premise for this type of power transmission is to use beam-forming or other directional antenna techniques to direct power to a combined rectifier/antenna unit (known as a "rectenna"). Current research on MPT has achieved relatively low efficiency rates, often less than 1% [8]. Additionally, microwave power transmission is limited by safety regulations set in the United States by the Federal Communications Commission (FCC). The FCC defines maximum permissible exposure rates for both the general public and for the workplace [9]. Guidelines based on these recommendations (intended for the communications industry, but applicable to all microwave applications) recommend power levels on the order 1 watt or less for a 3 foot dish antenna to keep exposure to acceptable levels more than one wavelength from the transmitting antenna [10]. While this limit could be exceeded by using the higher occupational exposure limits and by setting a

minimum approach distance that is greater than one wavelength from the charging device (likely 1 meter or more, depending on the frequency and power levels used), it is unlikely that MPT will be able to match the power transfer levels of near-field techniques, especially considering efficiency.

2.1.5 Laser Power Beaming

Laser power beaming utilizes laser light to transfer electrical energy from one place to another. It works on the same principles as solar power, using photovoltaic cells to generate electricity. The only difference is that, rather than collecting energy from the sun, energy from a source is used to generate a laser. The laser stimulates the photovoltaic cells, which generate electricity. Laser power beaming has a number of benefits. The narrow beam of the laser allows for energy transfer at long distances. The receiver consists only of a small photovoltaic array, allowing for easy integration even in compact devices. Unlike other methods of energy transfer, laser power beaming does not interfere with nearby radio signals. However, there are several severe limitations on transferring energy via laser.

First, the amount of power transferred is directly proportional to the power of the laser. This makes this method impractical for anything more that charging relatively small, lightly loaded devices. The more power the system requires, the larger and stronger the laser must be to sustain it. As the laser becomes more powerful, the overall system becomes prohibitively expensive. Additionally, having a large number of high power lasers would make the environment dangerous for human workers as those lasers could pose a serious threat of bodily harm.

Another limitation is the efficiency of modern photovoltaics. Current technology only allows for less than 20% efficiency on average, meaning that only 1/5 of the energy directed at a photovoltaic cell is converted into useable electrical energy. Certain types of photovoltaics, known as concentrator solar cells, can have efficiencies as high as 40%, but this still represents a prohibitive amount of energy loss. This also only represents losses on the receiving side of the transfer and does not take into account the efficiency of the laser emitter. This can vary greatly depending upon the laser design and output power. However, the higher the power of the laser, the less efficient the energy conversion process becomes.

2.2 Market

In recent years, markets of wireless charging have gradually grown as consumers are purchasing more electronic devices. According to the company IHS Technology, the wireless power market is expected to grow from $216 million in 2013 to $8.5 billion in 2018 [11]. This is due to an anticipated switch from wired to wireless technologies within many industries. For example, Thoratec, a healthcare company, is working with WiTricity on a wireless way to charge heart pumps and other medical equipment. Another example is, Lockheed Martin, the aerospace and defense giant. Lockheed is working on a laser-based system to recharge drones in mid-flight. This technology has helped industry to explore into new dimension which they contribute to the study of wireless power transfer.

2.3 Health and Safety Concerns

One of the biggest concerns of wireless power transmission is safety for the environment and for humans. Exposure to electromagnetic fields (EMF) is not a new phenomenon, but exposure to man-made electromagnetic fields has been steadily increasing as technologies and communication behavior have created more and more artificial sources. Currently there are multiple organizations studying the effects of EMF. Organizations such as the World Health Organization (WHO) [12], the International Commission on Non-Ionizing Radiation Protection (ICNIRP), National Institute for Occupational Safety and Health (NIOSH), and the Institute of Electrical and Electronic Engineering (IEEE) studied and formulated guidelines establishing limits of EMF exposure [4].

At the relatively low frequencies this project utilizes, RF safety is not a significant issue. At RF and lower frequencies, the primary health concern comes from heating due to EM wave absorption by the body. The amount of absorption is related to the wavelength of the EM wave relative to the body. At low frequencies, these wavelengths are on the order of hundreds of meters to kilometers. At these wavelengths, absorption levels are much lower than at frequencies where the waves are of similar wavelength to the human body. Frequencies below 100kHz are often below the threshold where specific exposure limits are defined, due to their low risk for adverse health effects.

2.4 Battery

One of the requirements of this project is to collect and store the energy from the wireless transfer. This portion of the requirement relies heavily on the battery. This is why it is important to research battery types and then select a battery that would be able to meet the requirements. The research involved exploring the variety of battery types and their characteristics such as energy density, cell voltage, load current, charge time, cost, and maintenance requirement. In the following subsections it will describe each of these parameters with their respective battery type.

2.4.1 Nickel Cadmium (NiCd)

Back before lithium ion batteries were introduced to the market, Nickel Cadmium (NiCd) and Nickel Metal Hydride (NiMH) were the battery types used in portable devices. Some positive characteristic of the NiCd battery is that it has a long cycle life, able to operate in varies temperature, fast charging time, and low price. The negative characteristic is that it has a low energy density, high self-discharge, and it does get affected by the memory effect. Memory effect occurs when a battery is repeatedly recharged before it has been completely discharged, which results the battery not to fully discharge its true capacity.

- energy density ranges from $45 - 80\frac{Wh}{kg}$
- cell voltage $1.25V$
- charge time 1 hour

- load current: $20A$ peak

2.4.2 Nickel-Metal Hydride (NiMH)

The NiMH rechargeable batteries are another popular type of batteries used in many applications such as digital cameras, GPS units, and MP3 players. Some advantages of NiMH are it high capacities, doesnâĂŹt get affected by memory effect compared to NiCd, simple to store, and environmentally friendly. The disadvantages are that its life cycle is than that to NiCd, high self-discharge, and requires maintenance.

- energy density ranges from $60 - 120\frac{Wh}{kg}$
- cell voltage: $1.25V$
- charge time: 2–4 hours
- load current: $5A$ peak

2.4.3 Lithium Ion (Li-Ion)

The lithium based batteries are one of the most powerful but yet dangerous type of batteries. The Li-Ion polymer batteries have the highest energy density than another battery which is why the electric vehicle industry is using this type of battery. Li-Ion has a low self-discharge, little to no maintenance, and a single cell has a potential energy of 3.7V. The negative side of the Li-Ion battery is that it is dangerous to overcharge and to expose it to hot environment. This is why it required having a protection circuit module (PCM) or a battery management system (BMS) for high voltage packs.

- energy density ranges from $100 - 130\frac{Wh}{kg}$
- cell voltage: $3.7V$
- charge time: 2–4 hours
- load current: $2A$ peak

Chapter 3

Methodology

We chose to implement the wireless charging system with resonant inductive coupling, as that appeared to be the most safe and efficient method of wireless power transfer. The scope of the project is limited to demonstration of the transfer system, so peripheral components such as a DC power supply, a load management system, or a computerized charging control system were not prototyped. A diagram of a complete implementation (excluding control systems) is shown in Figure 3.1.

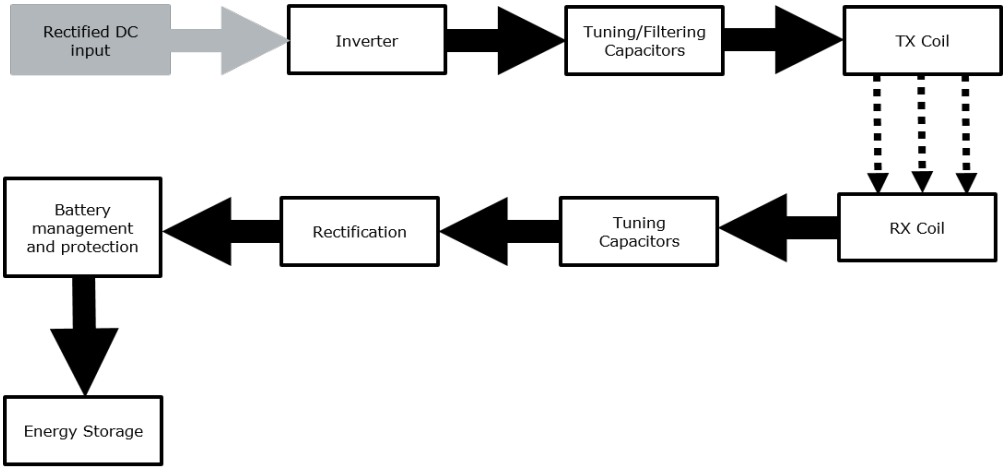

Figure 3.1: Block Diagram of Charging System

Chapter 4

Project Design

4.1 Transmitter

The transmitter power circuit takes 120V, 60Hz AC power from a standard wall outlet, and converts it to 50V, 10kHz AC power, suitable for transmission through the charging coils. A full block diagram of the circuit is shown in Figure 4.1.

4.1.1 Inverter

The inverter takes rectified DC power, and generates a 10kHz square wave to drive the coils. It is composed of four NMOS transistors in an H-bridge configuration, and a gate driver circuit. While 60 volts DC is specified in the schematics, the inverter can function with any voltage between 17 and 75 volts. This adjustable input voltage can be used to to calibrate the circuit for various operating distances, and possibly new coil designs, to ensure that the output voltage of the receive coil is sufficient to drive the load.

H-Bridge

An H-bridge is a configuration of four transistors connecting both sides of a load to the positive and negative voltage rails. By alternating the switching of opposing pairs of transistors, the H-bridge is able to reverse the current flow through the load, simulating an AC source.

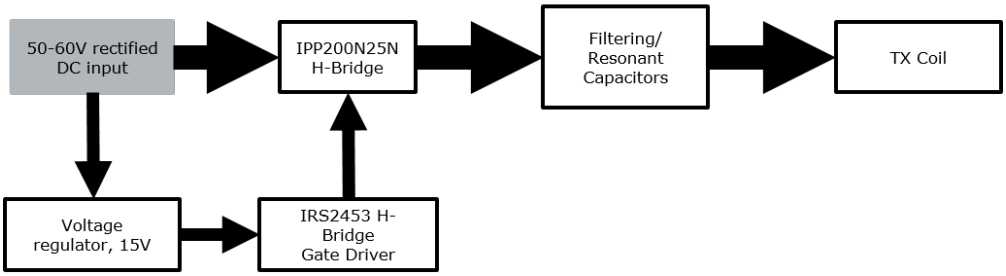

Figure 4.1: Block diagram of transmitter circuit

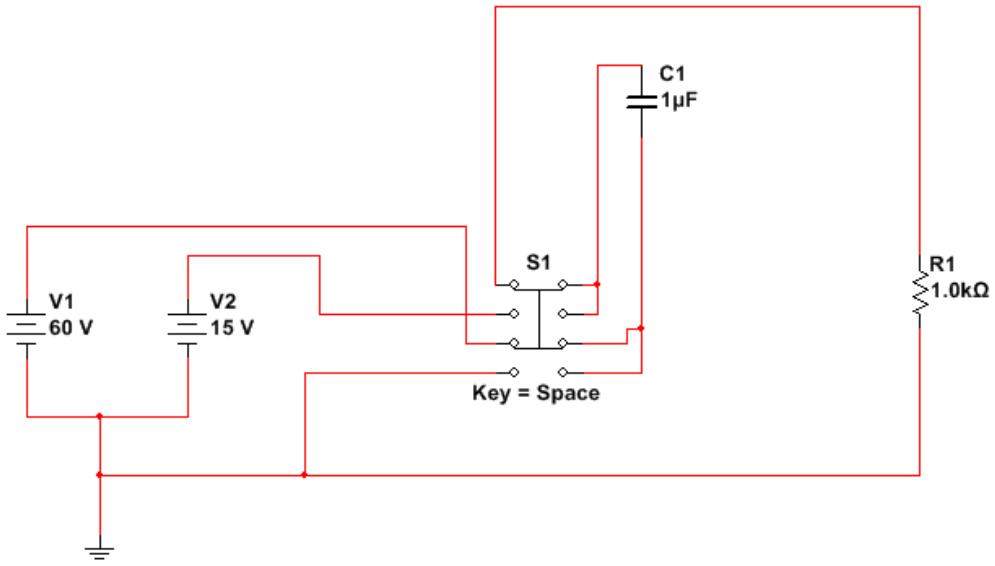

Figure 4.2: Simplified model of bootstrap capacitor MOSFET gate driver

The H-bridge used in this circuit consists of 4 Infineon IPP200N25N3 [13] transistors. These transistors were selected because they are rated to switch 250V and have a low drain to source resistance (R_{DS}). Due to the NMOS construction of these transistors, the gate pin must be driven at a higher voltage than the source pin. For the high side transistors, this requires a gate voltage higher than the high voltage supply. To achieve this high gate voltage, a gate driver circuit is employed.

Gate Driver

The gate driver provides appropriate current levels for the high and low side transistors of the inverter [14]. The gate driver selected for this circuit is the IRS245D [15], manufactured by International Rectifier. This gate driver circuit is designed to drive both the high and low side MOSFETs of an H-bridge. The IRS2453 has the ability to switch both the high and low side MOSFETs, and includes a timing circuit similar to the 555 timer.

Design Theory The IRS2453 gate driver employs a bootstrap capacitor to attain the voltage levels necessary to drive the high side transistors. These capacitors are C2 and C3 in the diagram in Appendix A. A bootstrap capacitor is charged from the 15 volt supply to the inverter circuit (through diodes D5 and D6). Once these capacitors are charged, the negative side of the capacitor is allowed to float to the voltage at the source of the driven transistor, forcing the high side of the capacitor to a level 15 volts higher than the source pin of the transistor, ensuring a sufficient gate voltage. Figure 4.2 illustrates a simplified layout of a bootstrap circuit.

Transient Elimination A limitation of the H-bridge configuration is the high $\frac{dv}{dt}$, which causes large voltage spikes during the turn-off of the transistors, due to stray inductances within the circuit. This is illustrated in Figure 4.3. To fix this, a snubber circuit was inserted

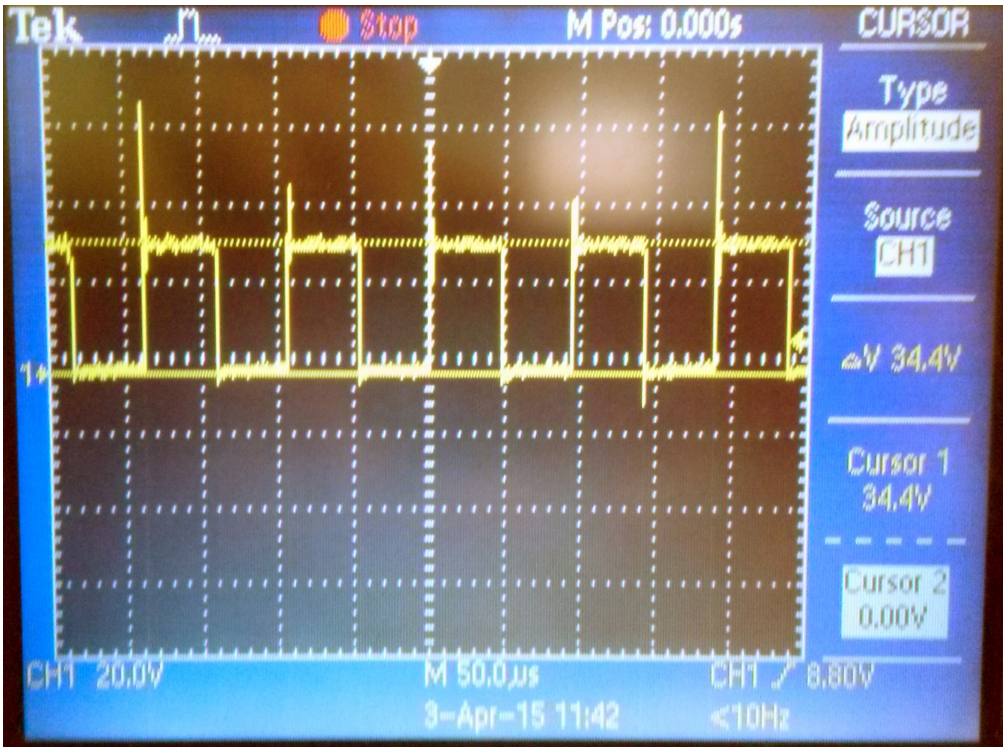

Figure 4.3: Transients in inverter switching

across the drain and source pins of each of the H-bridge MOSFETs (see Figure 4.5). The values of the capacitor and resistor were chosen empirically, using the smallest value capacitor and resistor that would provide sufficient transient suppression, as the power dissipation of the snubber is directly proportional to the capacitor value [16].

IRS2453 V_{cc} Supply While early testing was conducted supplying the IC from a 15V DC power supply that was separate from the high voltage supply, it is required that the IC and the transmitter coil receive power from the same source. As it is out of scope to build a DC power supply, an LM317HV [17] variable voltage regulator was chosen to create 15V DC from the high voltage supply. The output of this regulator is set by a resistive voltage divider, and can be adjusted through the use of a potentiometer included in the circuit.

4.2 Transfer Coils

The transfer coils form the core of the power transfer process. The coils are each wired in parallel with a capacitor such that they both have a resonant frequency of approximately $10kHz$. The coils also act as a 2:1 voltage transformer, transforming the $50V$ input waveform to a $25V$ peak output. Using ANSYS Maxwell (an electromagnetic field simulator) and a MATLAB script we experimented with various designs and orientations of coils and attempted to predict each design's efficiency.

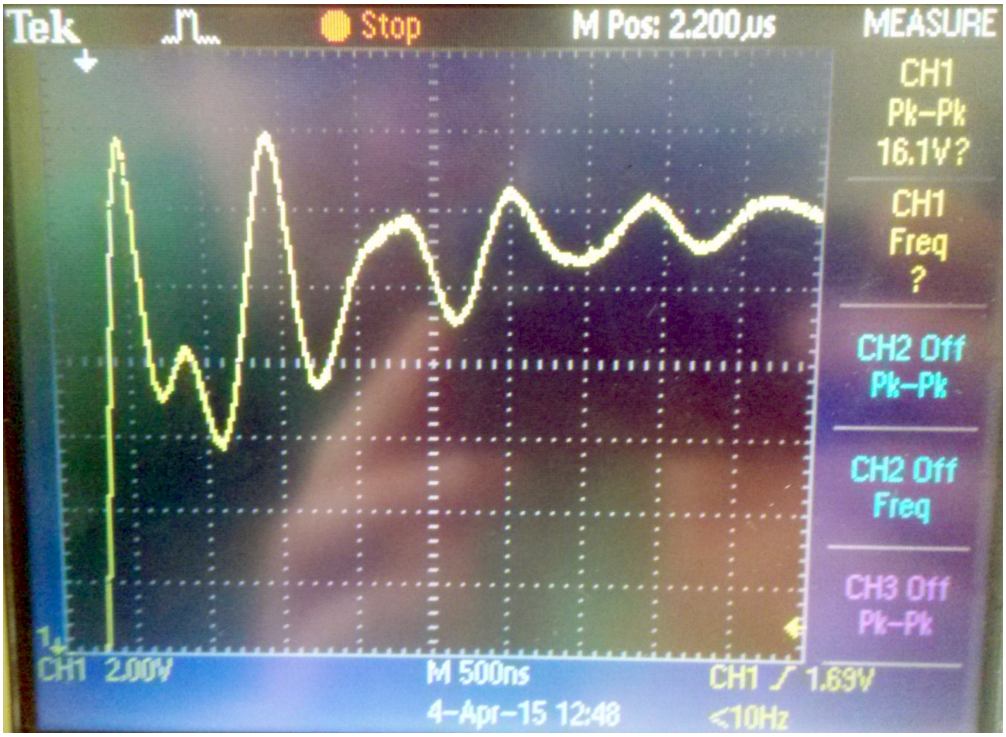

Figure 4.4: Transients in inverter switching (close up)

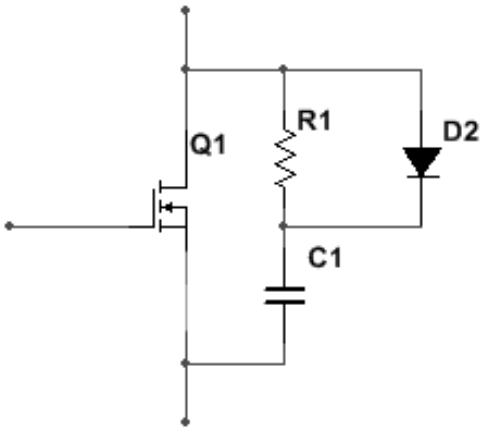

Figure 4.5: Ideal Snubber

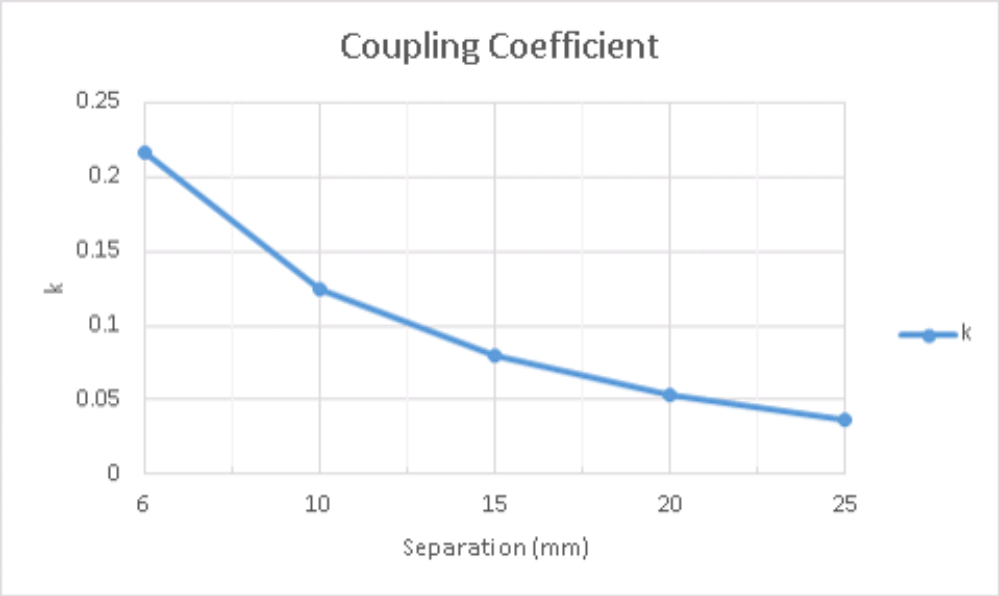

Figure 4.6: Simulation results

4.2.1 Intended Performance

At the start of this project, we had intended to achieve a peak overall efficiency of 75%. However, we quickly discovered that such efficiency was simply not possible. All of the testing and research that we did on the simulation coils indicated a maximum possible efficiency of 30% when the coils were separated by 2cm. However, this number represented ideal conditions, so we expected our actual efficiency to be somewhat less than 30%.

4.2.2 Simulation and Design Process

Using ANSYS Maxwell, we simulated various combinations of coil geometry and orientation in order to determine the coupling coefficient, k, in each case (Figure 4.6). The coupling coefficient is the ratio of the induced current in the receiver coil to the energizing current in the transfer coil. This has a direct effect upon the efficiency of the energy transfer process. Once we had determined the coupling coefficient using Maxwell, we were able to calculate estimated values for the inductances of both coils, and the transfer efficiency. We did this using a MATLAB script that applied the following equation:

$$\mu = (U^2)/(1 + \sqrt{1 + U^2}^2 \tag{4.1}$$

Where $U = k\sqrt{Q_1 Q_2}$. Q_1 and Q_2 are the quality factors of the two coils. They are calculated using the internal inductance, capacitance, and resistance of the LC circuits in accordance with the equation $Q = R^(- 1)\sqrt{L/C}$. R is negligible at resonant frequency, L can be calculated by Maxwell, and C is determined based on the desired resonance.

We also used the same script to calculate the coupling coefficient based on coil dimensions, separation distance, and overlapping cross-sectional area. We included this in the code because, for several weeks, we were unable to use Maxwell due to a technical problem.

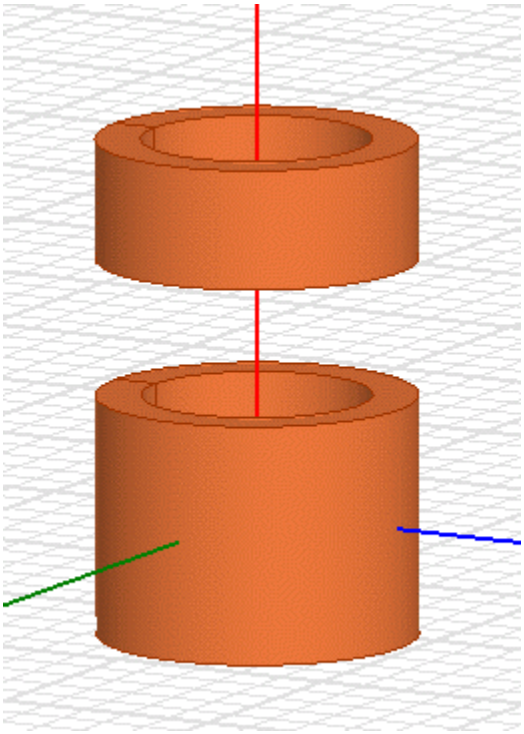

Figure 4.7: Coil Design in ANSYS Maxwell

4.2.3 Finalized Design

Following all this simulation and experimentation, we settled on a final design. The coils are each $1in$ in diameter, 3 layers thick, and oriented along the same axis. The Transfer coil has 16 turns per layer, and the Receiver coil has 8 turns per layer. Figure 4.7 depicts our finalized coil design in Maxwell.

4.3 Receiver Circuit

The main purpose of the receiver circuit is to transfer the power created by the transmitter magnetic field to the system/battery. In order for this circuit to work properly, there are stages to convert the 24 VAC 10 kHz input to a steady 12 VDC and supply this 12 VDC to the system/battery. Figures 4.8 and 4.9, presents an overview of the components used in order to achieve the desired voltage and current to power a 100 Watt load. The stages to convert AC to DC are rectifier and voltage regulator. The stage of storing the energy collected from the transfer process consists of a charge controller and a battery. These stages will be discussed more in-depth in the following subsections.

4.3.1 Rectifier

A rectifier is an electrical device that converts alternating current (AC), which periodically reverses direction, to direct current (DC), which flows in only one direction. The process is known as rectification. Physically, rectifiers take a number of forms, including solid-state

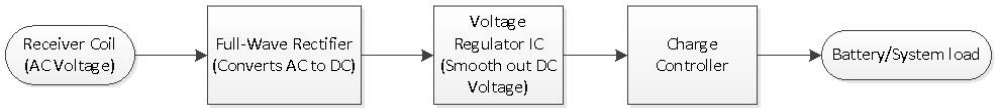

Figure 4.8: Block diagram of the receiver circuit

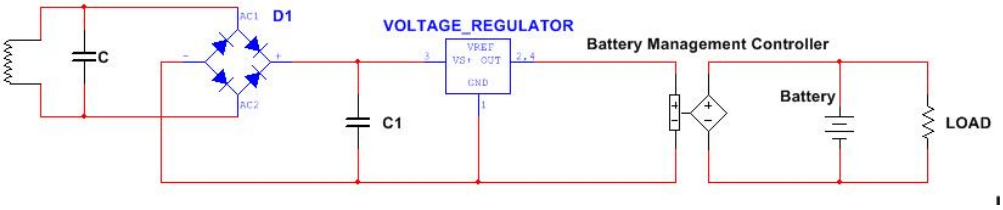

Figure 4.9: Circuit overview of the receiver circuit

diodes, silicon-controlled rectifiers and other silicon-based semiconductor switches [18]. A full-wave bridge rectifier is an arrangement of four diodes in a bridge circuit configuration that provide a desired output, Figure 4.10. The essential feature of a full-wave bridge rectifier is that the polarity of the output is the same regardless of the polarity at the input.

The operation of the bridge rectifier is as follows:

1. In the positive half cycle of the AC sine wave signal, diodes D1 and D2 are in forward bias and will conduct while diodes D3 and D4 are reverse biased. The current will flow through diodes D1 and D2.

2. In the negative half cycle, diodes D1 and D2 are now in reverse biased and diodes D3 and D4 are in forward bias. The current flows through D3 and D4

In Figure 4.11, is a simulation of a full-wave rectifier with an input of 24 V_{RMS} 10 kHz, which is the intended voltage captured from the transmitter, and a 5Ω load. For the full-wave bridge rectifier, Schottky diodes are used instead of regular diodes due to their low voltage drop, approximately 0.3V per diodes ($4 * 0.3V_{DROP} = 1.2V_{DROP}$). In the oscilloscope view

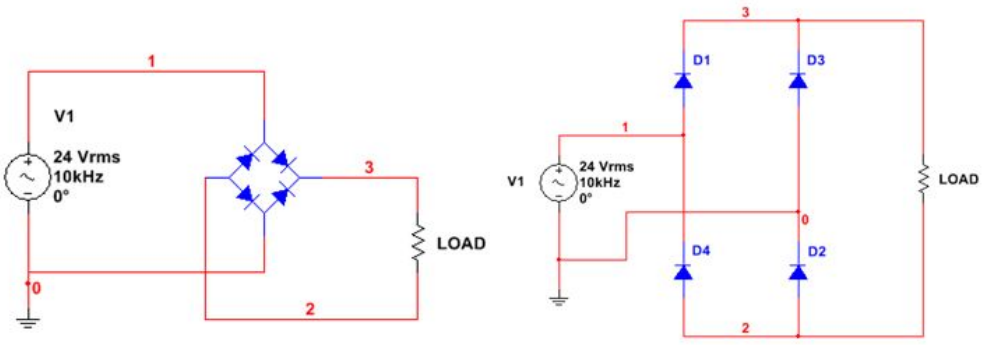

Figure 4.10: Full wave bridge rectifier circuit

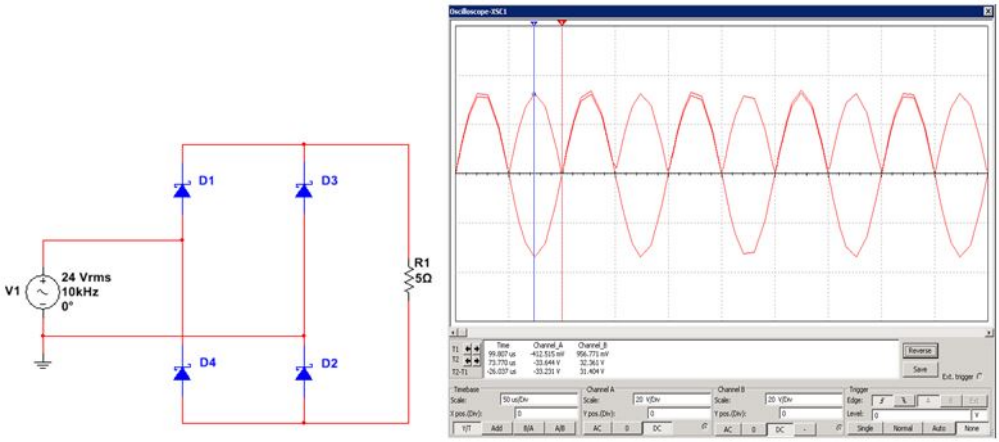

Figure 4.11: Simulated full wave bridge rectifier circuit and oscilloscope of V1 and voltage output

it is noticeable how the full-wave rectifier converts the sine wave of the AC input to a DC output.

In order to reduce the ripple of the output voltage, a capacitor is placed in parallel to the resistive load, Figure 4.12. Initially, as the output voltage of the rectifier rises to its peak voltage, the capacitor would charge to the peak output voltage. As soon as the source decreases the capacitor will discharge to the load resistor and start charging again as the output voltage rises again in it 2/period. Picking the right value capacitor is extremely important in order to achieve a nearly smooth pure DC. The equation for this is the following:

$$C = \frac{1}{2fr(\Delta V_0/V_m)} \tag{4.2}$$

$$\begin{aligned} \text{Where} \ : C &= \text{capacitance} \\ f &= \text{frequency} \\ r &= \text{Resistance} \\ (\Delta V_0/V_m) &= \text{ratio of ripple voltage} \end{aligned}$$

Using this equation, a $1mF$ capacitor or higher is ideal to maintain a nearly pure DC.

$$C = \frac{1}{2fr(\Delta V_0/V_m)} = \frac{1}{(2(10^4))(5)(0.01)} = 0.001F \tag{4.3}$$

4.3.2 Voltage Regulator IC

A voltage regulator is an electrical device designed to automatically maintain a constant voltage level. A voltage regulator may be a simple feed-forward design or may include negative feedback control loops. Depending on the design, it may be used to regulate one or more AC or DC voltages. In this project, a MIC29502WT voltage regulator IC was used. The reason MIC29502WT is picked is for three reasons,

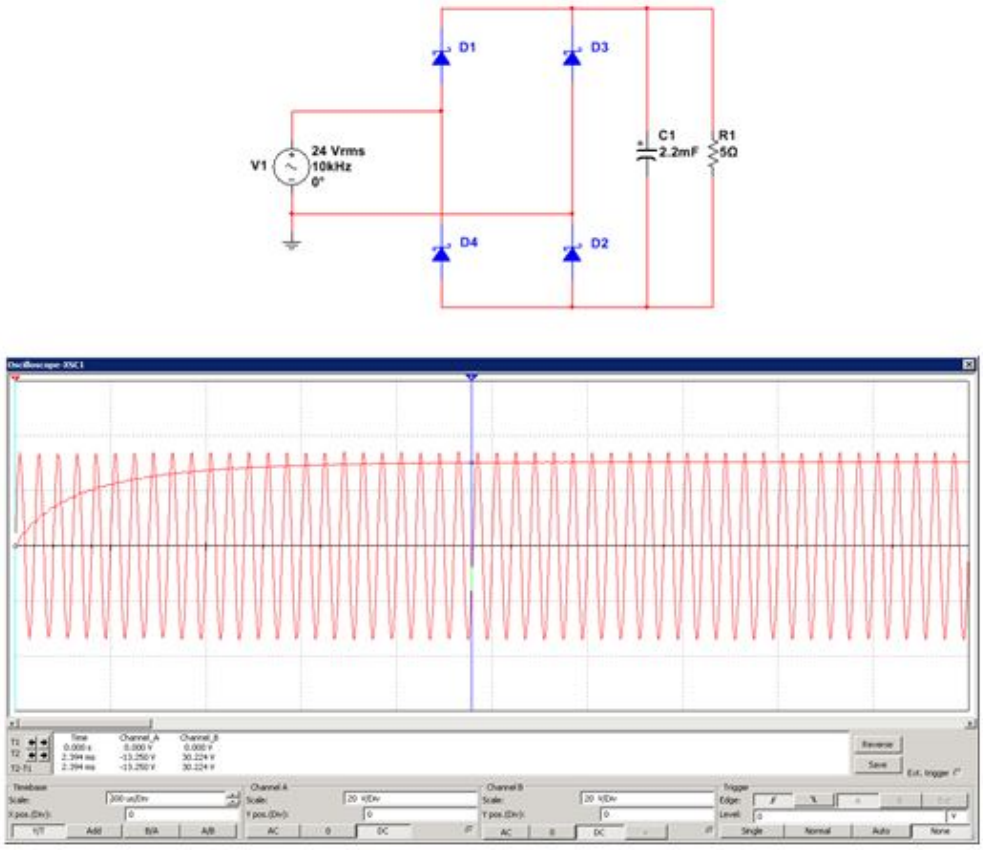

Figure 4.12: Full wave rectifier with a smoothing capacitor and oscilloscope view

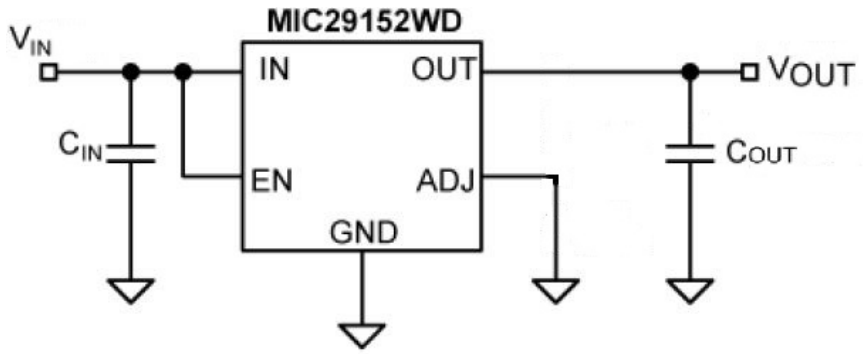

Figure 4.13: Voltage regulator schematic

- The output voltage is adjustable ($1.25VDC$ $26VDC$)
- Outputs up to 5A
- Low voltage ($0.37V$@$5A$)

This voltage regulator gives the flexibility of adjusting the output voltage from the range of 1.25V to 26V. The flexibility is great because the same regulator can be used in case some modification is made to the battery/system in the future. Figure 4.13 presents a schematic of the MIC29502WT. The values of the capacitors are recommended values based of the datasheet and their values are as follows:

- C_{IN}: 10uF
- C_{OUT}: 10uF

4.3.3 Battery Management System

The purpose of a battery management system is to regulate the current flowing into the battery. This acts as a charge protection for the battery as it prevents overcharge and it monitors the batteries charge level. This is an important component in this design because the Li-Ion batteries require a protection circuit to maintain voltage and current within a safe limit.

The battery managements system used is a MCP73842. The MCP73842 is an advance dual cell lithium-ion linear charge management controller. This charge controller provides high accuracy, constant-voltage, constant-current regulation, cell preconditioning, cell temperature monitoring, advance safety timer, automatic charge termination, and charge status indicator. The MCP73842 is designed to operate in conjunction with either a host microcontroller or in stand-alone application. The circuit below is provided by datasheet Figure 4.14.

The values of the components are the following:

- C_1: 10uF

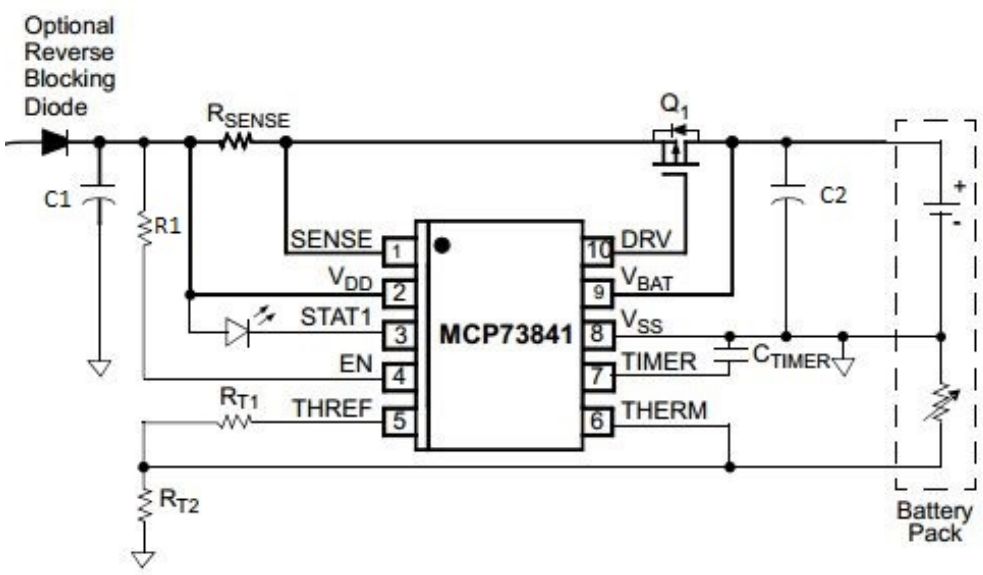

Figure 4.14: Battery management schematic

- C_2: 4.7uF
- C_{timer}: 0.1uF
- Q_1: IRLIB9343
- R_1: $100k\Omega$
- R_{sense}: 0.2Ω
- R_{T1}: 187Ω
- R_{T2}: 195Ω

Some of these components values were recommended by the datasheet of the MCP73842, C_1, C_2, C_{timer}, and R_1. Other components such as R_{sense}, R_{T1}, and R_{T2} were calculated based on equations provided by the datasheet [19]. R_{sense} is a sense resistor which regulates the rate of the charge current to the battery. This is calculated by the following equation:

$$R_{sense} = \frac{V_{FCS}}{I_{REG}} \tag{4.4}$$

Where $R_{sense} =$ Sense resistor
$V_{FCS} =$ Fast charge current regulation threshold (120mV)
$I_{REG} =$ Desired fast charge current in amp (600mA)

R_{T1} and R_{T2} are for the battery cell temperature sensor. These resistor values are calculated with the following equations:

$$R_{T1} = \frac{2R_{cold}R_{hot}}{R_{cold} - R_{hot}} \tag{4.5}$$

$$R_{T2} = \frac{2R_{cold}R_{hot}}{R_{cold} - 3R_{hot}} \tag{4.6}$$

Where R_{cold} and R_{hot} are the thermistor resistance values at the temperature. These were measured by heating up and cooling down the thermistor and measure these two temperature with a digital multimeter.

Chapter 5

Assembly

5.1 Transmitter

The assembly of the transmitter circuits was a two-stage process. First, the circuit was prototyped on a breadboard (see Figure 5.1 the breadboard prototype of the inverter). This prototype was powered via the bench power supply and connected to a high impedance load. After all troubleshooting and extensive testing was completed to verify the proper operation of the circuit, the circuit was transferred to a perforated board and soldered together for high power testing. The move away from a breadboard for high power testing was necessary because the tracks in the breadboard are unable to safely handle the high currents in parts of the circuit.

The circuit layout on the perforated board (shown in Figure 5.2) was designed to minimize connecting wire lengths and overlaps. This resulted in a fairly compartmentalized layout, with the supporting circuitry for the transistors (the snubbers and the gate resistors) clustered next to the transistors. The other major consideration during the circuit layout was the orientation and location of the transistors. All four H-bridge transistors were located at the edge of the board, where they could be attached to a heat sink if it were deemed necessary during testing.

5.2 Transfer Coils

For low power testing, the coils were placed on two seperate breadboards, with capacitors in parallel to create a resonant LC circuit, as illustrated in Figure 5.3.

5.2.1 Winding The Coils

We wound the coils using 18AWG wire, a hand-made jig (Figure 5.4), and a two-part epoxy glue. We used PVC pipe as the base for each coil and used wooden washers, clamped in place, in order to limit the number of turns per layer that we could wind. After winding each layer, we applied epoxy and allowed the coil to sit for some time before starting the next layer. However, the coils we were able to produce are far from perfect. It was very

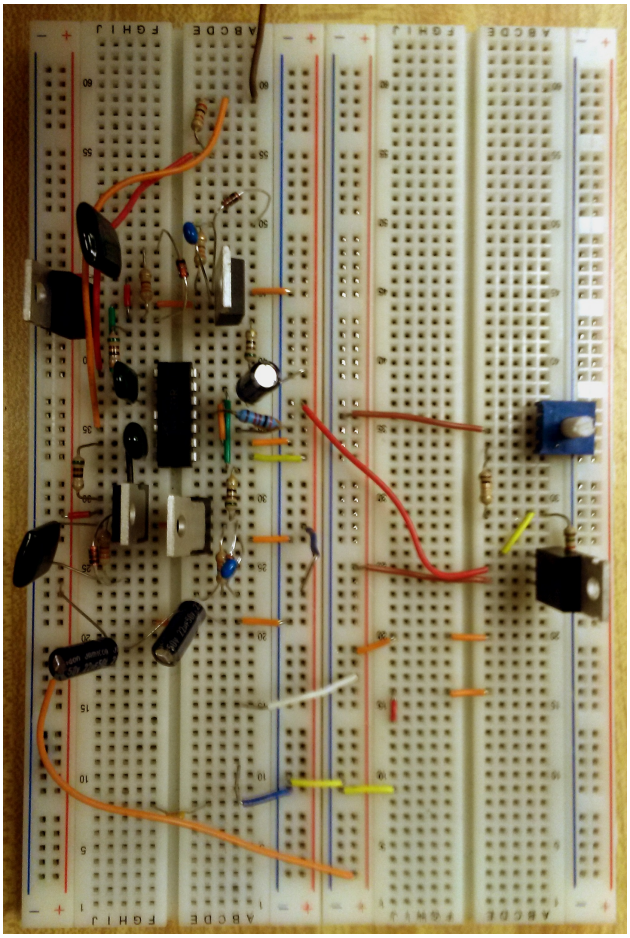

Figure 5.1: The current inverter design iteration assembled on a breadboard

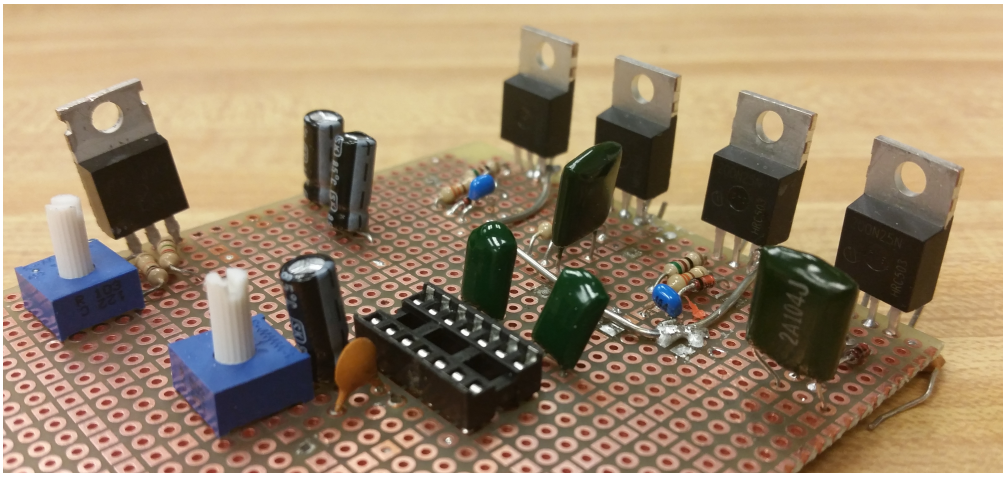

Figure 5.2: The current inverter design iteration assembled on a perforated board

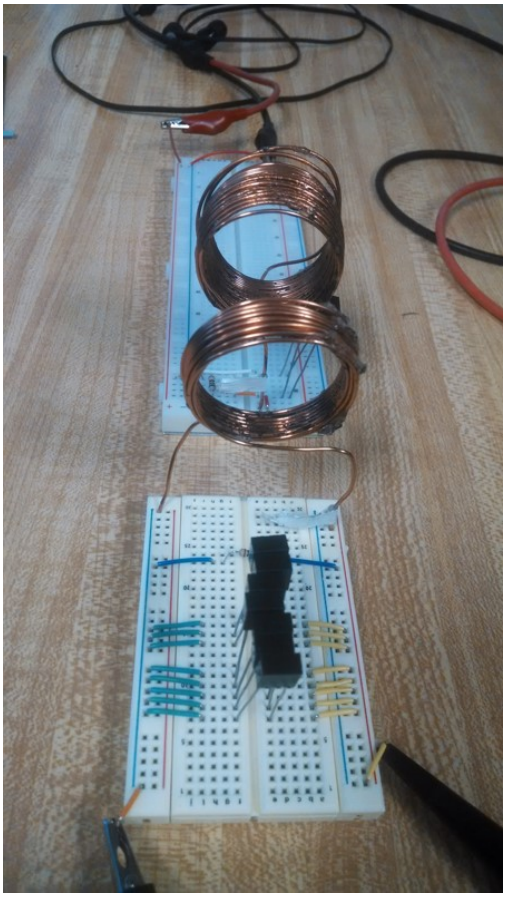

Figure 5.3: Low power testing of transfer coils

difficult to maintain the correct number of turns per layer using our jig. Additionally, the epoxy does a sufficient, but not perfect, job of holding the turns in place without a core.

Figure 5.4: Coil Winding Jig

Chapter 6

Results

6.1 Transmitter

6.1.1 Full-Power Inverter

Much of the project was spent troubleshooting iterations of the inverter circuit, including replacing multiple defective gate driver ICs and modifying component values. The primary issue experienced during the troubleshooting phase of the circuit was an inability of the circuit to generate high-side switching waveforms at voltages higher than the chip supply voltage of 15 volts. This culminated on rebuilding the circuit on a separate breadboard. The issue briefly reappeared on the new breadboard, but was quickly solved by replacing the IC.

As expected and illustrated in Figure 6.1, the circuit produced a square wave with a peak-to-peak voltage similar to the high voltage input (30 and 60 volts during testing). The results were obtained using a $2k\Omega$ load, pending transfer to a perfboard for full power testing.

Unfortunately, the seventh and final spare IRS2453 failed shortly before the results were obtained from full-power testing using the board shown in Figure **??**. Due to project time constraints, it was not possible to procure additional IRS2453 samples for further testing. However, since full-power testing of the coils was an important component of the project, an alternative circuit was developed. This circuit, which can supply 10 Watts (not the 100 Watts that the full-power inverter could supply, but still sufficient to produce meaningful test results) is described in the section 6.1.2.

6.1.2 Medium Power Inverter

Due to the untimely failure of the IRS2453 IC used in the full power inverter circuit, an alternative inverter circuit needed to be constructed with parts on hand to obtain the results expected from full power testing. After a survey of available parts, it was concluded that it would not be possible to fully replace the IRS2453 to conduct full power testing at 100 Watts.

Fortunately, a Texas Instruments SN754410NE Quad Half-H Driver [20] was available. This IC contains four outputs that can be switched between ground and a voltage of up to 36 volts, supplying a maximum of 1 amp of current. To create a proper H-bridge inverter using this chip, two outputs needed to be used, and switched with complementary square

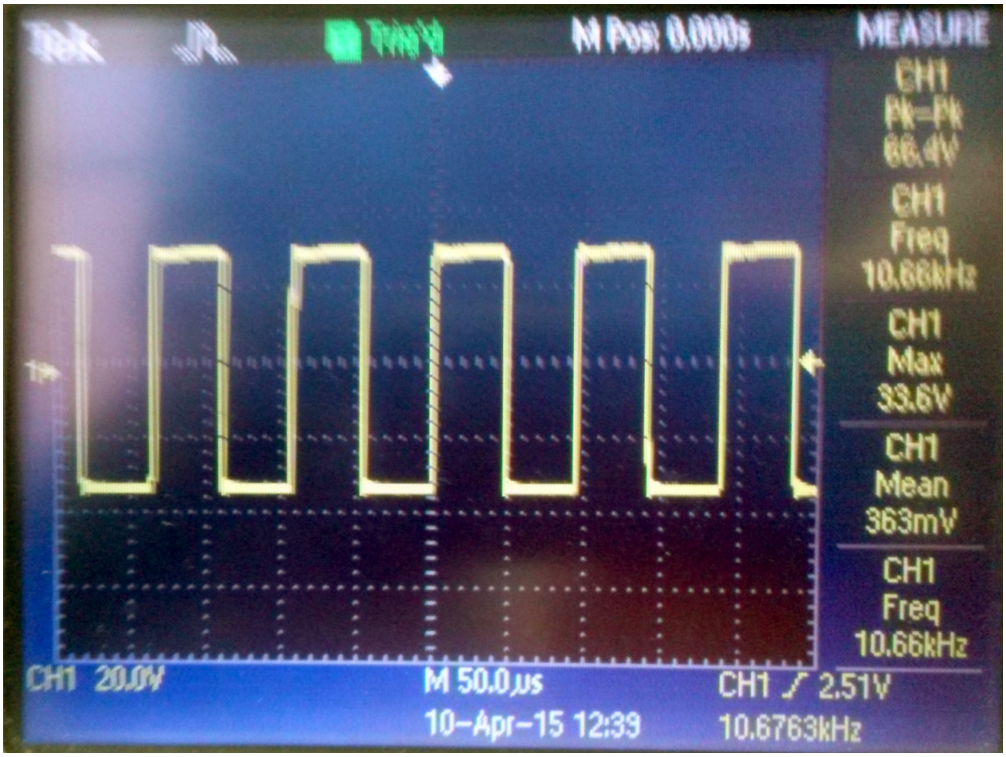

Figure 6.1: Output voltage of inverter across high impedance resistive load

wave inputs. An appropriate square wave (0–5 volts, at the resonant frequency of the coils) was generated with a function generator. This square wave directly controlled one half of the H-bridge, wile the other half of the H-bridge was controlled by a complementary square wave generated by a logic inverter circuit connected to the function generator square wave. The logic inverter was created by connecting all the inputs of a 4 input NAND gate on a HEF4012B [21] IC, as this chip was on hand. An alternative IC, such as a 4011 2 input NAND gate or any suitable logic inverter or NOT gate IC can be substituted if available. The circuit diagram is shown in Figure 6.2 and the circuit as built is shown in Figure 6.3.

Figure 6.4 shows the output of the inverter with no load. For coil testing, a 10Ω, 10 Watt resistor was used as a load, meaning the inverter voltage was limited to 10 Volts to stay within the specifications of the H-bridge chip.

6.2 Transfer Coils

We collected data on the coils performance prior to assembling the overall device at very low power. The coils and capacitors were arranged on breadboards and used the function generators available in the lab as a power supply. After the low power test was completed, we soldered the coils and capacitors into the transmitter and receiver circuits in order to run full power tests on the whole circuit.

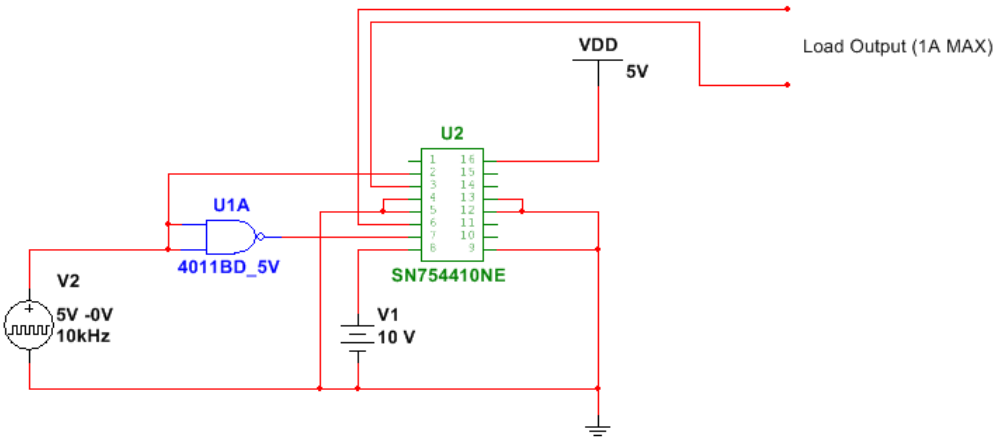

Figure 6.2: Circuit diagram of medium power inverter

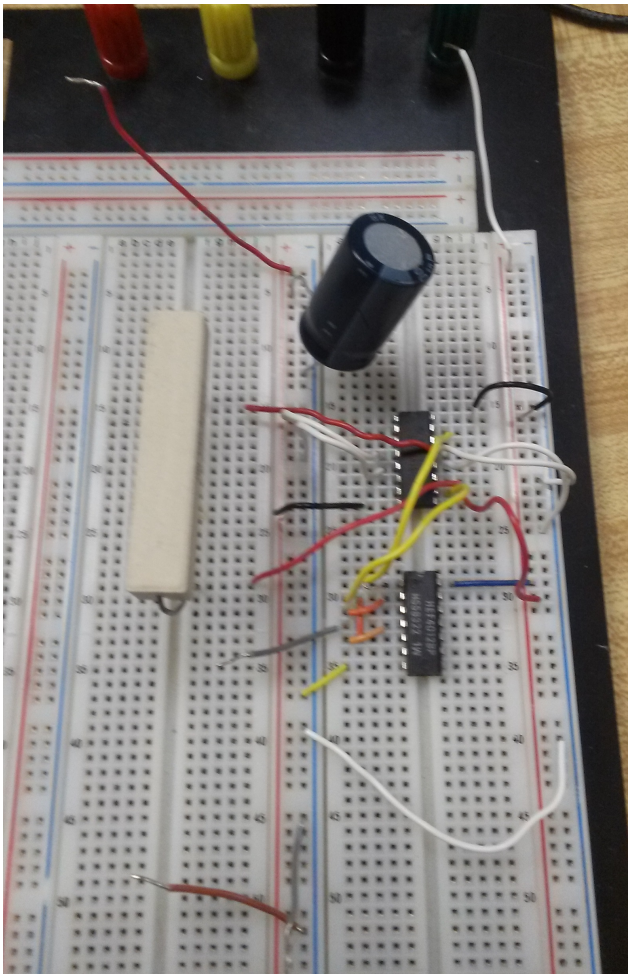

Figure 6.3: Breadboard prototype of medium power inverter

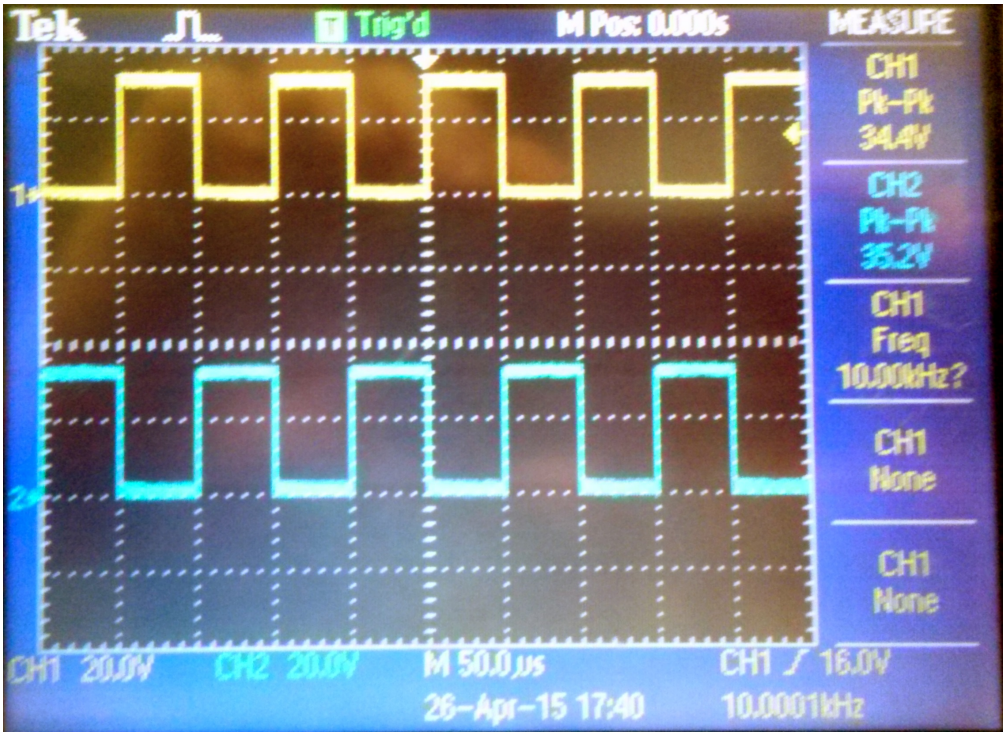

Figure 6.4: No-load output of medium power inverter

6.2.1 Low Power Testing

Using a function generator allowed us to run tests isolating the coils and capacitors, but imposed strict power limitations. The function generator's maximum output power is dependent upon the function frequency. So, our first test was to determine the exact resonant frequency of the coils. To do this, we swept the frequency up from 6-12kHz for both the transmitter and receiver in order to find the resonant frequency of each LC pair. At resonant frequency, impedance is at its lowest, thus the output voltage of the sample LRC circuit is at its highest. In each coil, we measured the resonant frequency at 9.5kHz.

At this frequency, the function generator's maximum power supply is just under $60mW$ at $1.02V_{PK}$. Even though this is less than 1000th of the power supply we expect in the final build, it is still a good indicator of how the coils will perform.

Next, we tested the performance of the coils without the capacitors (i.e. without resonant coupling) in order to illustrate the potential of this method of energy transfer. At a separation distance of $5mm$, the non-resonant coils had a maximum efficiency of 0.01%. At the same distance, with resonant coupling, we measured a maximum efficiency of 19%.

After discovering the resonant frequency and establishing a non-resonant baseline, we calculated the power outputs for a range of separation distances and offsets in order to calculate the efficiency in each case. We took measurements at separation distances of $5mm$, $15mm$, $25mm$, $35mm$, $45mm$, and $50mm$. Additionally, we measured the performance of the coils at offset distances of $0mm$(coils fully overlap), $8mm$, $16mm$, and $32mm$(coils do not overlap at all) when at separations of $5mm$, $25mm$, and $50mm$. At each position, we

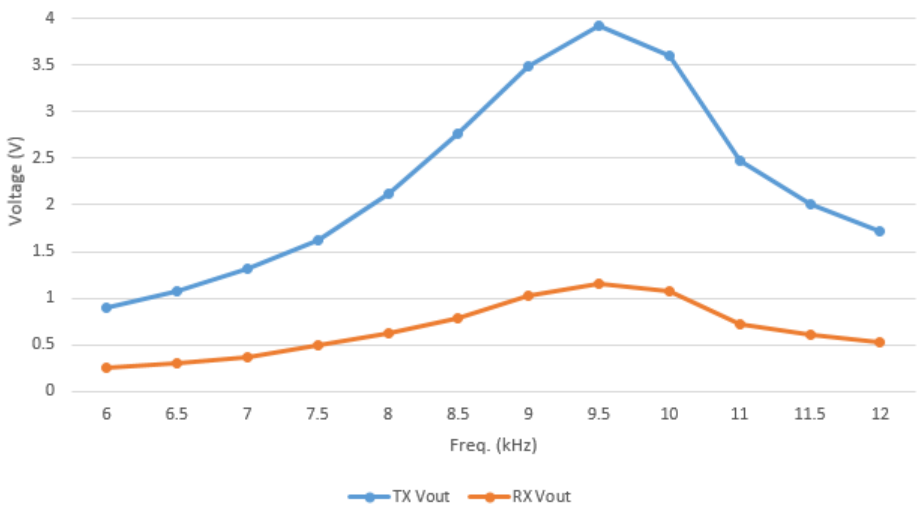

Figure 6.5: Output Voltage of Transmitter and Receiver as a function of Frequency

measured the receiving coil's output voltage, V_{out}, with a load of 10.05Ω. We then used the following formulas to calculate rated power,P_{actual}, as well as efficiency. Table 6.2.1 contains the results at each position.

6.2.2 Mid-Power Testing

We next used a mid-power transmitter circuit to test the coil performance. The configuration of the transmitter circuit allowed us to use the function generator to determine the waveform and frequency of the output signal, but drew the power from the Lab DC power supply. Figure 6.8 shows the output voltage waveform in blue and the voltage drop across a 10.05Ω resistor in yellow. The voltage drop is important because it allows us to determine the input current to the transmitter coil. The peak current is determined by the equation $I_{pk} = 0.9V/10.05\Omega$ This gives us $I_{pk} = 89.56mA$. The peak power in the transmitter coil is thus such that $P_{TXmax} = V_{in} * I_{pk} = 7V * 89.56mA = 0.627W$

However, this does not accurately represent the average power of the system. To determine this, we measure the area under the voltage drop curve for one cycle and divide by the cycle length. Doing this, we found that we had an average voltage drop of 146mV. We then repeat the previous calculations to solve for $P_{TXavg} = 102mW$.

The next step was to calculate the power delivered to the load resistor from the receiver coil. Figure 6.9 shows the output waveform from the Receiver coil to the load resitor at a separation of 10mm and 0 offset. It is interesting to note that, while the waveform at the transmitter coil was a square wave, the waveform at the receiver coil is a sinusoidal wave. This is because the sinusoidal function at the receiver is composed of the fundamental frequency of the input square wave. The other composite frequencies of the square wave have been largely filtered out because they are not at resonant frequency. To calculate the power output, we used the equation, $P_{out} = V_{rms}/(R^2_{load})$. We then calculted efficiency by comparing the power out to the power in. Figure 6.10 shows the details of the output power and efficiency that we calculated as separation and offset varied. Figures 6.11 and 6.12

Sep. (mm)	Offset (mm)	P_{out}	Efficiency
5	0.0	11.8	0.19
	8.0	10.2	0.17
	16.0	5.73	0.10
	32.0	1.43	0.02
15	0.0	3.82	0.07
25	0.0	1.34	0.02
	8.0	0.99	0.017
	16.0	0.57	0.009
	32.0	0.27	0.005
35	0.0	0.39	0.007
45	0.0	0.17	0.003
50	0.0	0.11	0.002
	8.0	0.11	0.002
	16.0	0.08	0.001
	32.0	0.07	0.001

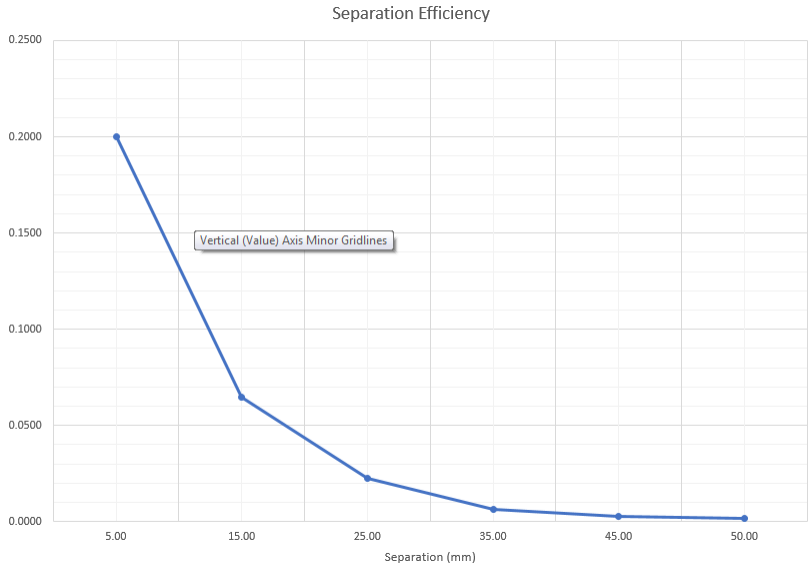

Figure 6.6: Plot of Efficiency as a function of Separation at 0 Offset

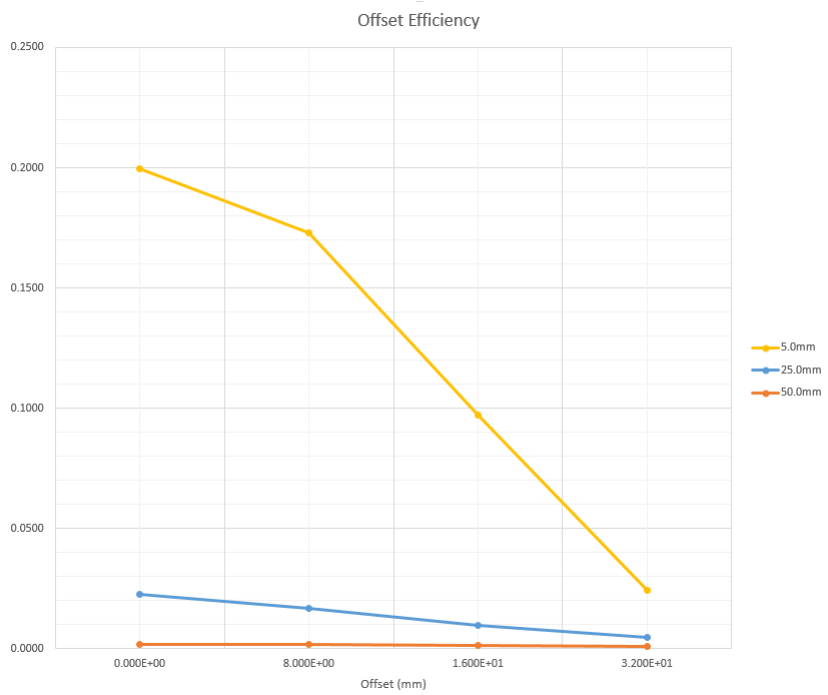

Figure 6.7: Plot of Efficiency as a function of offset at Separation distances of 5mm, 25mm, and 50mm

demonstrate the effect of separation and offset. Interestingly, these results are very similar to the results that we received in the low-power test.

6.3 Receiver Circuit

The receiver circuit, as previously mentioned, consists of a rectifier, voltage regulator, charge controller, and battery/system load. The rectifier and voltage regulator portion of the circuit were order and assembled on a breadbroad as shown in Figure 6.13. To test this circuit it was connected to a function generator which outputs 10V at 10 kHz. Even though the initial input is 24 VAC at 10 kHz, it is very difficult to obtain this condition on a function generator, which is why 10V is used.

For the full-wave rectifier circuit, LQA05TC600 Schottky diodes were used for the rectification due to their low voltage drop characteristic and its ability to handle 5 amps at 600V. Figure 6.14, shows how these diodes performance when 120 Hz and 10 kHz are inputted. With 120 Hz the bridge rectifier successfully produced a rectified DC voltage, while with 10 kHz it has a bit of a distortion but it still outputs a DC source. This distortion is due to its slow reverse recovery time, which will be ignored once a capacitor is place in parallel to the load resistor.

In Figure 6.15, a steady 10.6VDC is produced when a 2.2 mF capacitor is placed in parallel to the load resistor. This output voltage is then filtered through the voltage regulator in which it outputs a pure 10VDC. This circuit demonstrated a success in converting 10VAC at 10 kHz to 10VDC. This output voltage will go to the battery charge controller where it

Figure 6.8: Graphs of the output signal to the transmitter coil (Blue) and the voltage drop across a 10Ω output resistor (Yellow)

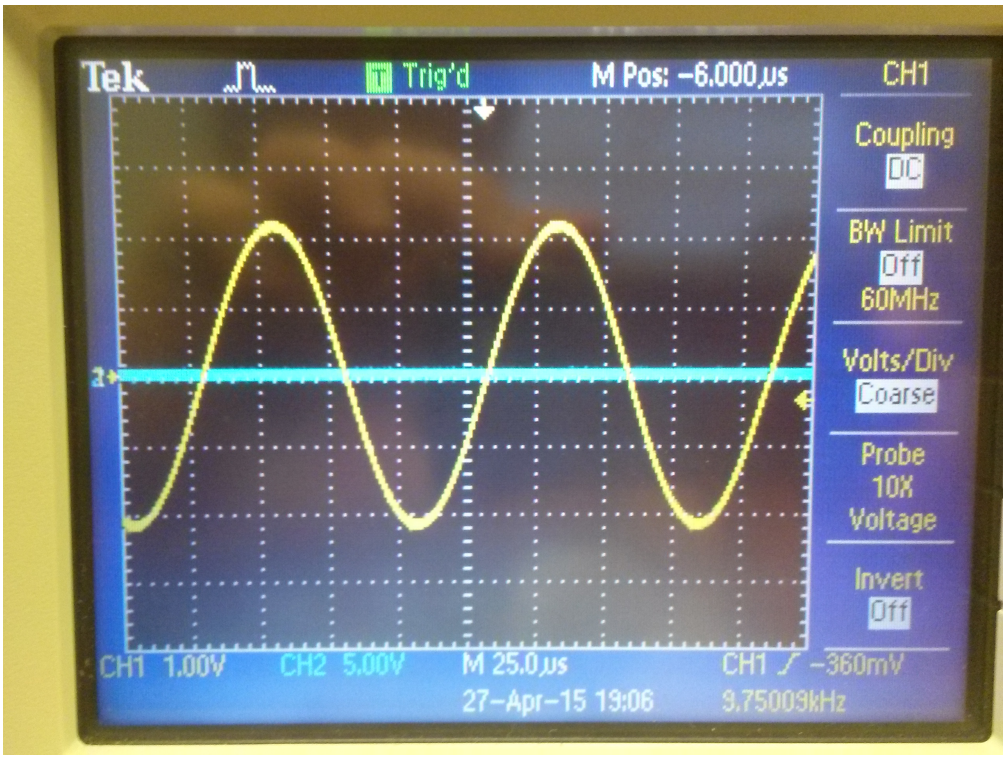

Figure 6.9: Graph of the output voltage from receiver coil across 10Ω load resistor

Sep (mm)	offset (mm)	Pout (W)	Efficiency
10	0	0.01648721	0.161639317
	8	0.015634424	0.153278663
	16	0.012933932	0.126803257
	32	0.009522785	0.09336064
	40	0.005756311	0.056434417
20	0	0.009949179	0.097540967
30	0	0.005685245	0.055737696
40	0	0.003411147	0.033442617
50	0	0.002025369	0.019856554

Figure 6.10: Chart detailing output power and efficiency at various coil positions

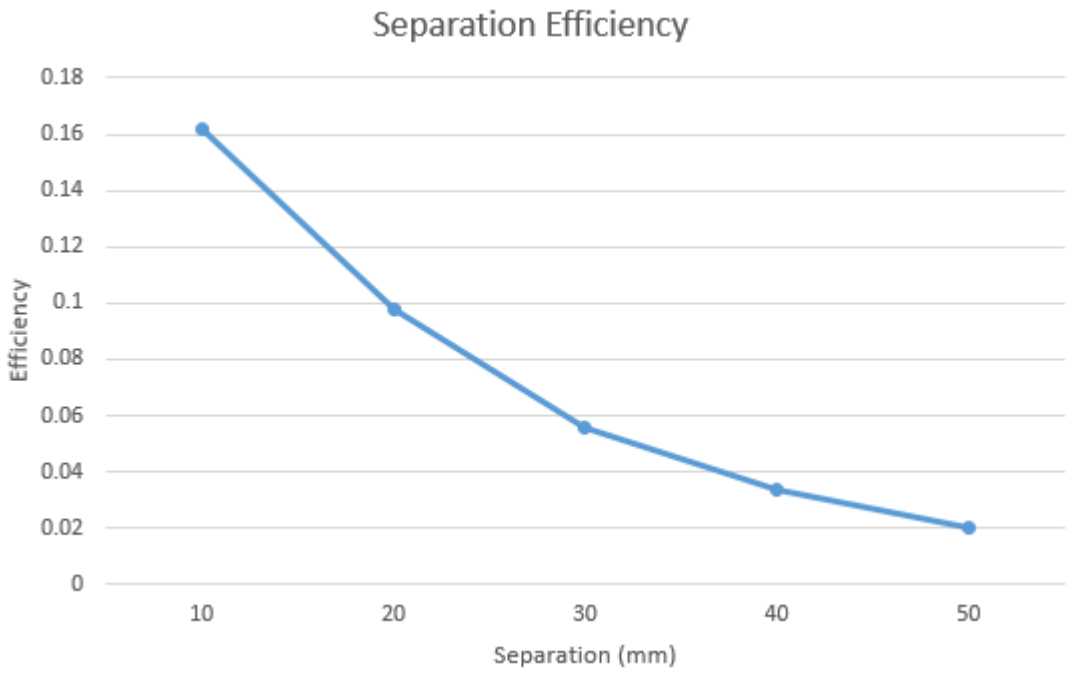

Figure 6.11: Graph of Efficiency as separation increases

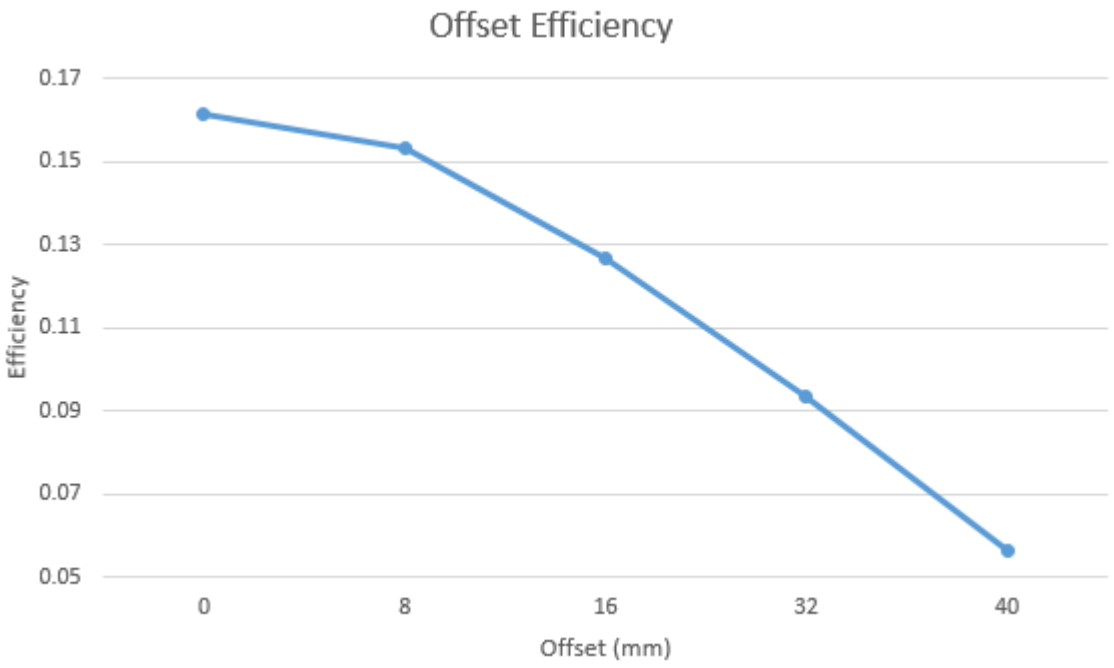

Figure 6.12: Graph of efficiency as offset increases

should charge a Li-ion battery. The charge controller will be ordered over winter break and tested with this circuit.

6.3.1 Battery Management System

To test if the battery management circuit worked properly a series of test were performed. The first test consisted of connecting the already fully charged battery to the battery management circuit and by using a bench power supply inputted a range of voltages from 8.9V to 12V. This test expects the battery management circuit to cut power to the battery since it is fully charged and the LED indicator should be off. The results were positive since the LED indicator was in fact off and by using a digital multimeter the output of the battery management circuit to the battery measured to 0V. For the second test, the thermistors were disconnected from the circuit. With the thermistor disconnected the LED indicator should be blinking indicating an issue and the result was a success. The third test consisted of charging the battery, in order the perform this test the battery was discharged by connected it to a load in series to a LED. The initial voltage of the battery was 7.4V and after the discharge it was 6.8V. Once the battery was connected the to the management circuit the LED indicator turned on, which is a positive result. The voltage output was 8.4V and the management circuit supplied 1A at the output. The last test consist of manipulating the thermistor resistance by heating the thermistor. To perform this test the thermistor was removed from the battery pack. Then the battery was connected back to the management circuit for it to continue charging. With the thermistor away from the battery, the temperature was taken by a digital multimeter which was able to measure the temperature since it had a thermocouple. The initial temperature was $74°F$ with a resistance of 12 ohms.

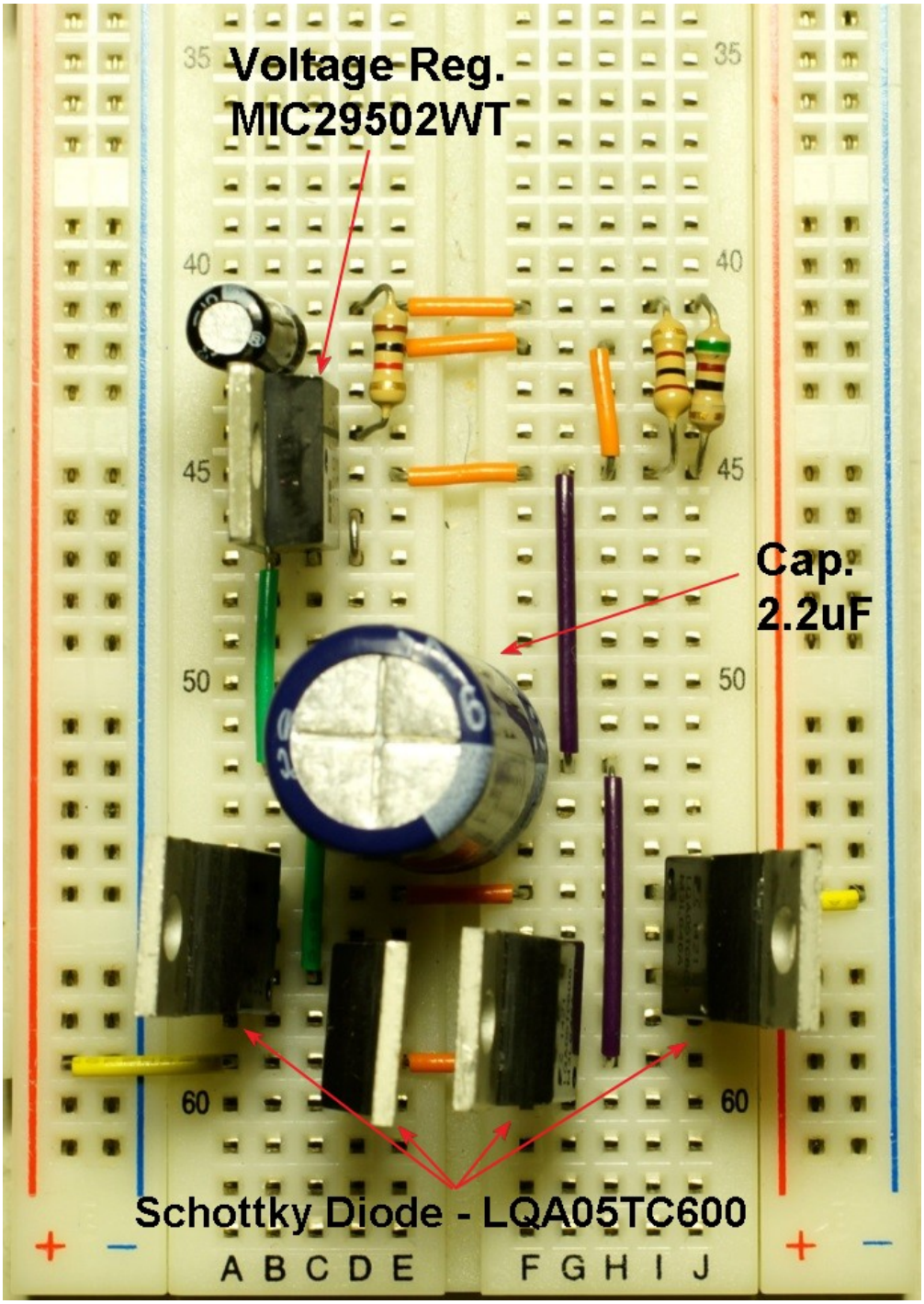

Figure 6.13: Receiver Circuit with 1 kâĎę load

Figure 6.14: Oscilloscope view of diodes rectifying 120 Hz(left) and 10 kHz (right)

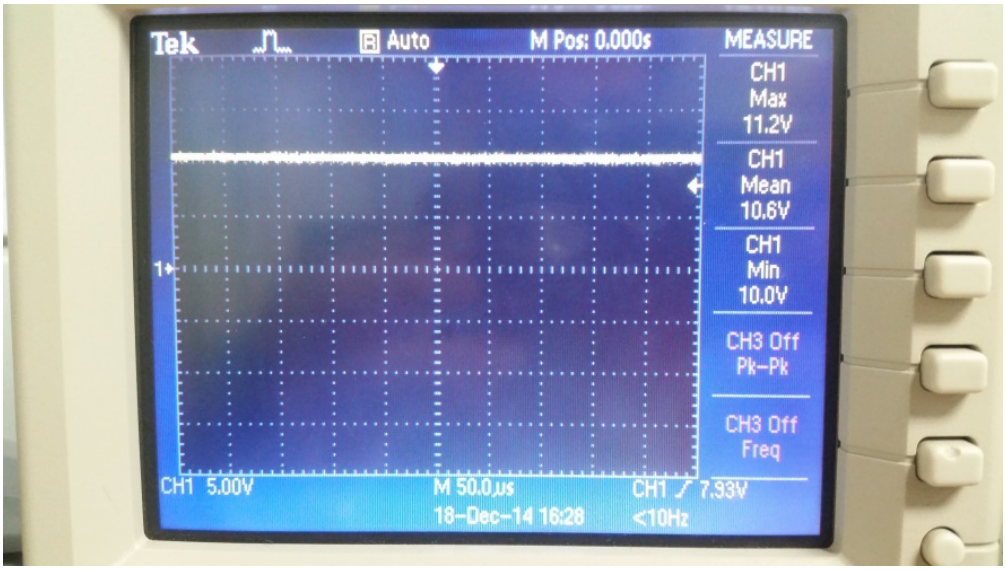

Figure 6.15: Pure 10 VDC with 2.2mF smoothing capacitor

To increase the temperature a soldering iron was placed near the thermistor and when the temperature reached $110°F$ the management circuit cut-off power to the battery, which is a positive result. During these test some safety precautions were taken due to the volatility of the lithium ion battery. These precautions consist of wearing safety glasses, working in a well ventilated area, and having a fire extinguisher near by.

Chapter 7

Conclusion

Through the design and testing of the wireless charging prototype, it was determined that wireless power transfer can be conducted at useful levels, but efficiency still poses a major challenge. Before this technology is employed to widespread commercial use, much more research and development is required. Resonant coupling seems to be a promising technology to achieve wireless power transfer.

References

[1] S. Åăarboh, "The patents of nikola tesla," *World Patent Information*, vol. 32, no. 4, pp. 335–339, December 2010.

[2] A. R. Hambley, *Electrical Engineering: Principles and Applications*, 4th ed. Upper Saddle River, N.J: Pearson Prentice Hall, 2008.

[3] M. G. Egan, D. L. O'Sullivan, J. G. Hayes, M. J. Willers, and C. P. Henze,

[4] N. Chawla and S. Tosunoglu, "State of the art in inductive charging for electronic appliances and its future in transportation," *2012 Florida Conference on Recent Advances in Robotics*, May 2012.

[5] R. M. J. D. J. AndrÃĺ Kurs Aristeidis Karalis and M. S. Peter Fisher, "Wireless power transfer via strongly coupled magnetic resonances," *Science*, vol. 317, pp. 83–85, June 2007.

[6] M. Kline, "Capacitive power transfer," M.S. thesis, University of California at Berkeley, Berkely, CA, 2010.

[7] W. C. Brown and E. E. Eves, "Beamed microwave power transmission and its application to space," *IEEE Transactions on Microwave Theory and Techniques*, vol. 40, no. 2, pp. 1239–1251, 1992.

[8] M. Ishiba, J. Ishida, K. Komurasakil, and Y. Arakawa, *Wireless power transmission using modulated microwave*, Conference Paper, Uji, Kyoto, Japan, 2011.

[9] J. Cleveland Robert F., D. M. Sylvar, and J. L. Ulcek, *Evaluating Compliance with FCC Guidelines for Human Exposure to Radiofrequency Electromagnetic Fields*. Washington, D.C.: Federal Communications Commission Office of Engineering & Technology.

[10] M. Butcher, *Microwave point-to-point antennas and rf safety*, Pamphlet, 2012. [Online]. Available: `http://www.sitesafe.com/PDFs/Microwave%20Point-to-Point%20Antennas%20and%20RF%20Safety-PE.pdf`.

[11] *Global market revenue for wireless charging to rise by nearly factor of 40 by 2018*, Web Page, 2014. [Online]. Available: `http://press.ihs.com/press-release/design-supply-chain/global-market-revenue-wireless-charging-rise-nearly-factor-40-2018`.

[12] "WHO | standards and guidelines," *WHO*, 2014. [Online]. Available: `http://www.who.int/peh-emf/standards/en/`.

[13] *Opti-MOS 3 Power-Transistor*, Rev. 2.4, Infineon, Jul. 2011.

[14] "Application note: An-937: Gate drive characteristics and requirements for HEXFET Power MOSFETs."

[15] *IRS2453(1)D(S)*, International Rectifier, Nov. 2012.

[16] *Snubber circuit design - practical tips*, Web Page, 2015-04. [Online]. Available: `http://www.ti.com/ww/en/analog/power_management/snubber_circuit_design.html`.

[17] *LM117HV/LM317HV 3 Terminal Adjustible Regulator*, SNVS773C, Rev. C, Texas Instruments, Apr. 2013.

[18] D. W. Hart, *Power Electronics*. 1221 Avenue of the Americas, N.Y: McGraw-Hill, 2011.

[19] *MCP73841/2/3/4 Advanced Single or Dual Cell Lithium-Ion/Lithium-Polymer Charge Management Controllers*, DS21823D, Microchip Technology Inc, 2013.

[20] *Quadruple Half-H Driver*, SLRS007B, Rev. B, Texas Instruments, Nov. 1995.

[21] *Dual 4-input NAND Gate*, Phillips Semiconductors, Jan. 1995.

Appendix A

Full-Power Inverter

Parts List

Quantity	Reference	Description
4	R1, R2, R3, R4	Resistor, 51Ω, $0.25W$, 5%
1	R6	Resistor, $1.5k\Omega$, $0.25W$, 5%,
1	R7	Resistor, $10k\Omega$, $0.25W$, 5%,
4	R9, R10, R11, R12	Resistor, 330Ω, $0.25W$, 5%
1	R5	$50k\Omega$ trim potentiometer
1	R8	$10k\Omega$ trim potentiometer
4	U1, U2, U3, U4	IPP200N25N3 PowerFET
1	U5	IRS2453D Gate Driver [15]
1	U6	LM317HV Voltage Regulator [17]
4	D1, D2, D3, D4	1N4148 Diode
1	C1	$2.2nF$ capacitor
2	C2, C3	$0.1\mu F$ capacitor
4	C4, C5, C6, C7	$100nF$ capacitor

Circuit Diagram

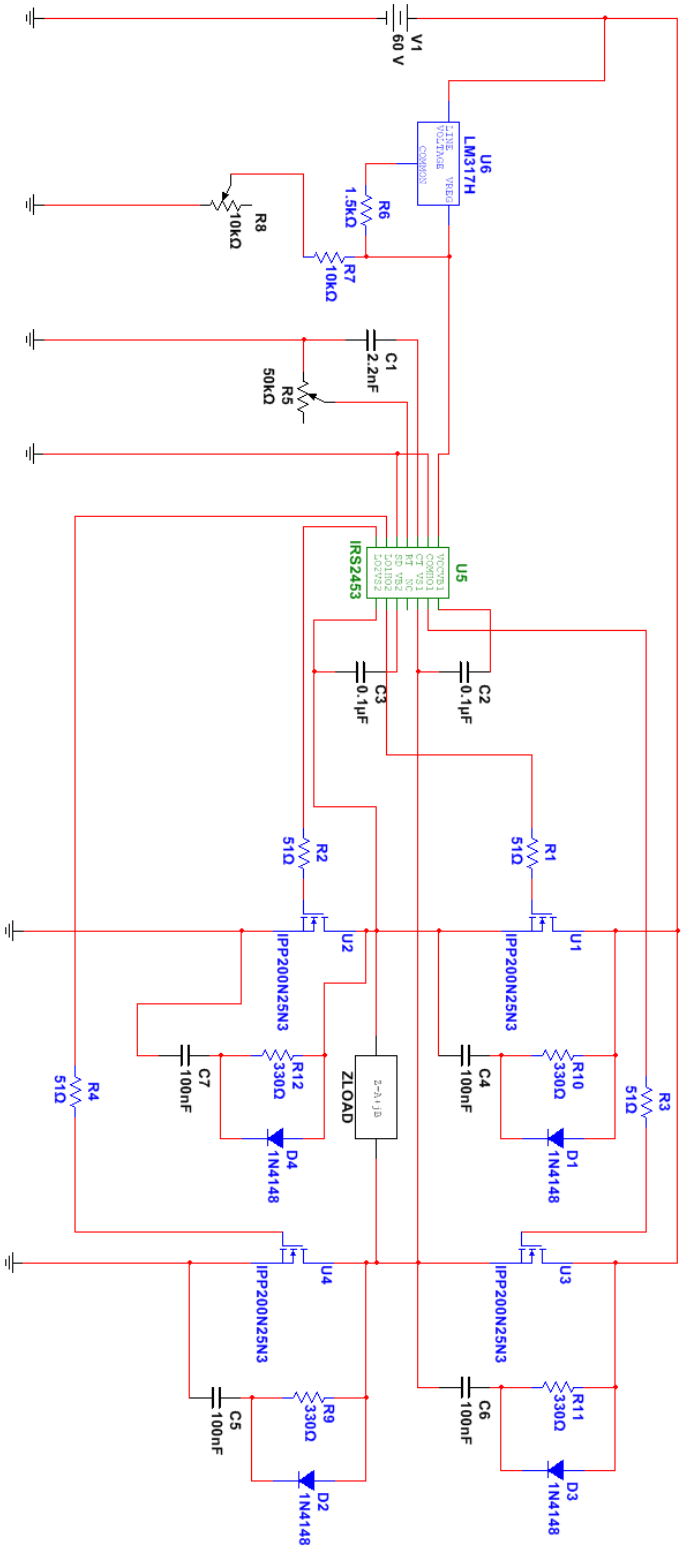

Theory of Operation

The inverter circuit provides alternating current to the load Z_{LOAD} by periodically switching the load terminals between the positive supply voltage (V_1) and ground. During half of the cycle, Z_{LOAD} is connected to V_1 through U_1, and to ground via U_4. During the other half of the cycle, Z_{LOAD} is connected to V_1 through U_3, and to ground via U_2. The IRS2453 H-bridge gate driver IC controls the switching of all four NMOS transistors of the H-bridge, and provides "dead time," in which none of the transistors are driven, between the halves of the cycle to inhibit a low impedance current path between V_1 and ground through a single side of the H-bridge. The frequency of oscillation is set via the resistor R_5 and the capacitor C_1. The inverter can switch a voltage of between approximately 14 volts to approximately 75 volts, with the voltage regulator U_6 representing the limiting component.

Adjustments

This circuit has two field adjustable settings: IC supply voltage and inverter output frequency.

IC Supply Voltage

The IC supply voltage (V_{CC}) can be adjusted via the $10k\Omega$ trim potentiometer R_8. This trim pot should be set to its minimum value, and then adjusted up until the IC supply voltage (measured at pin 2 of the LM317 voltage regulator U_6 or at pin 1 of the IRS2453 gate driver U_5) is between 12 and 14 volts. This should be adjusted before the first use of the circuit, and should not need to be readjusted to account for varying supply voltage.

Inverter Frequency

The inverter frequency can be adjusted using the $50k\Omega$ trim potentiometer R_5. This should be adjusted so the frequency of the output matches the resonant frequency of the transmitter coil. The range of adjustment allows for frequencies between approximately $5kHz$ and $100kHz$.

Appendix B

Receiver Circuit

Parts List

Quantity	Reference	Description
4	D1, D2, D3, D4	LQA05TC600 Schottky Diodes
1	C1	$2.2\mu F$ capacitor
2	C2, C3	$10\mu F$ capacitor
1	U1	MIC29502 Voltage Regulator

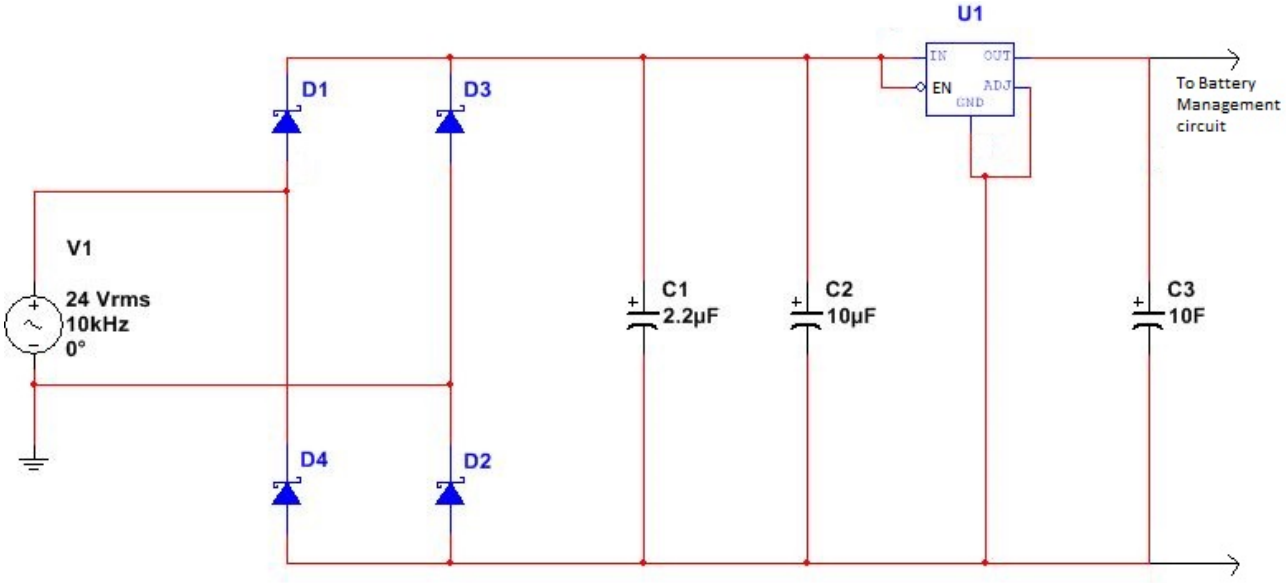
U1
IN
OUT
EN
ADJ
GND
To Battery
Management
circuit
D1
D3
D4
D2
V1
24 Vrms
10kHz
0°
C1
2.2µF
C2
10µF
C3
10F

Parts List

Quantity	Reference	Description
1	D1	LQA05TC600 Schottky Diodes
1	C1	$10\mu F$ capacitor
1	C2	$4.7\mu F$ capacitor
1	C_{TIMER}	$0.1\mu F$ capacitor
1	R_{Sense}	Resistor 0.2Ω
1	R1	Resistor $100k\Omega$
1	R_{T1}	Resistor 187Ω
1	R_{T2}	Resistor 195Ω
1	R_{TH}	NTC Thermistor 12Ω
2	LED	Green and Red LED's
1	Q1	IRLIB9343 P-Channel MOSFET
2	BATT	Lithium Polymer 3.7V, 5Ah
1	U1	MCP73841 Battery Management IC

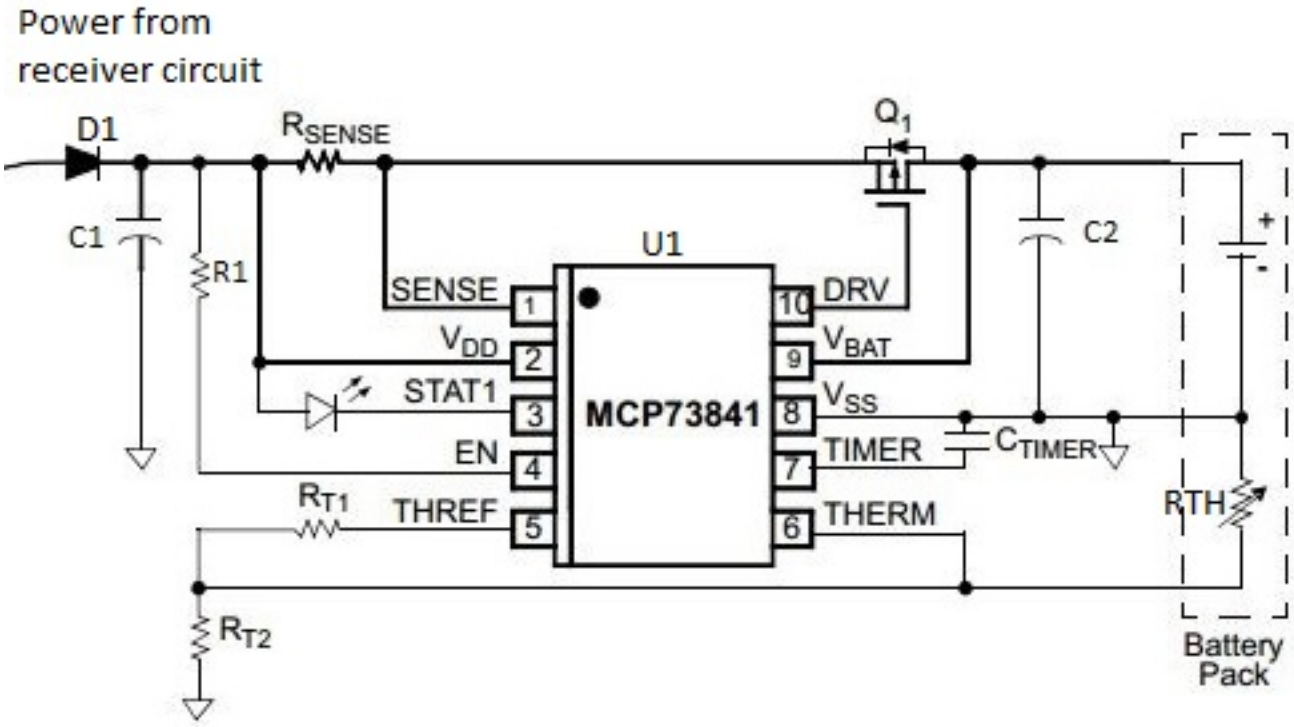
Power from
receiver circuit
D1
C1
R1
RSENSE
Q1
U1
SENSE
VDD
STAT1
EN
RT1
THREF
MCP73841
DRV
VBAT
VSS
TIMER
THERM
CTIMER
C2
RTH
RT2
+
-
Battery
Pack

Appendix C

MATLAB Code: Efficiency Calculations

```
%% Equations For Calculating the Efficiency of Resonantly Coupled %%
%% Inductive Power Transfer Coils

%%PHYSICAL PROPERTIES

%TX Coil
La1=3; %number of layers
N1=16; %number of turns per layer
d18=1.024*10^(-3); %diameter of 18AWG (m)
i1=3; %current (A)

IR1=16.7*10^-3; %inner Radius, m
OR1=IR1+2*d18*La1; %outer Radius, m
A1=pi*((2*d18*La1+2*IR1)/2)^2; %cross-sectional area (m^2)
le1=N1*d18; %length of coil (m)

%RX Coil
La2=3; %number of layers
N2=8; %number of turns per layer
i2=6; %current

IR2=16.7*10^-3; %inner Radius, m
OR2=IR2+2*d18*La2; %outer Radius, m

A2=pi*((2*d18*La2+2*IR2)/2)^2; %cross-sectional area (m^2)
le2=N2*d18; %length of coil (m)

%%INDUCTANCE CALCULATION
u0=(4*pi)*10^(-7); %vacuum permeability
ur=1; %relative permeability of air
```

```
a1=IR1+(OR1+IR1)/2;
b1=d18*N1;
c1=OR1-IR1;

a2=IR2+(OR2+IR2)/2;
b2=d18*N2;
c2=OR2-IR2;

%Welsby's Formula
%Inductance of primary coil (H)
L1=((u0*N1^2*pi*a1^2)/b1)*(1+0.9*a1/b1+0.32*c1/a1+0.84*c1/b1)^-1;
%Inductance of secondary coil (H)
L2=((u0*N2^2*pi*a2^2)/b2)*(1+0.9*a2/b2+0.32*c2/a2+0.84*c2/b2)^-1;

%%COUPLING COEFFICIENT

k=0.216; %Coupling Coefficient (unitless)

%%CIRCUIT INTEGRATION
f = 10000; %Resonant Frequency, Hz

C1 = (L1*(2*pi*f)^2)^-1; %Resonant Capacitance of L1, uF
C2 = (L2*(2*pi*f)^2)^-1; %Resonant Capacitance of L2, uF

R1 = 1; %series resistance for L1, Ohms
R2 = 1; %series resistance for L2, Ohms

%%EFFICIENCY CALCULATION
Q1 = (1/R1)*sqrt(L1/C1); %Quality Factor of Transfer circuit
Q2 = (1/R2)*sqrt(L2/C2); %Quality Factor of Reciever circuit

U = k*sqrt(Q1*Q2);

mu = (U^2)/((1+sqrt(1+(U^2)))^2); %Efficiency


%Output Following Values:

L1
L2
C1
C2
mu

%END
```

Appendix D

Buck Converter

The buck converter described in this appendix was part of an earlier system design, and would have provided the DC input into the inverter. The initial design, presented below, was designed to output a voltage of 55 volts (this voltage was increased to 60 volts after the buck converter was abandoned, in order to account for system losses and ensure an appropriate output voltage to the coils) to a 100 Watt load. It was discovered during prototyping that the converter as designed would not handle small loads appropriately without a greatly increased inductor value. Simultaneously, it was determined that the available lab bench power supply could supply appropriate DC power to the inverter, leading to the decision to remove the buck converter from the scope of the project. This appendix is provided for reference purposes only.

D.1 Design

The buck converter in the power path provides a 50V output to the inverter. The buck converter creates a reduced output voltage by switching the input source, and using the inductor and capacitor to store energy while the voltage source is connected, and provide energy to the load when the voltage source is disconnected. The diode provides an alternative current path when the voltage source is disconnected. A diagram of the buck converter circuit is shown in Figure D.1.

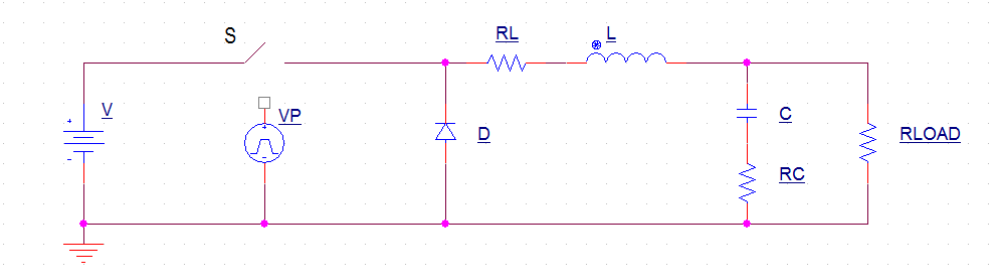

Figure D.1: Schematic diagram of buck converter.

Both buck converters can use the same design, varying the duty cycle of the input voltage switching to adjust the output voltage. The duty cycle and operating frequency will most likely be controlled by a 555 timer circuit and a power MOSFET, as yet to be selected.

D.1.1 Component Selection

The selection of component values for the buck converter is a straightforward, established process. The first parameter to be established is the duty cycle, which is the ratio of the output voltage to the input voltage. For this application, the input voltage was 120 volts, and the output voltage was selected to be 55 volts (D=0.458).

$$D = \frac{V_{OUT}}{V_{IN}} \tag{D.1}$$

The next step is to calculate the minimum inductance, according to the equation below, where f is the operating frequency, and R is the load impedance. With a switching frequency of 10kHz, and a load impedance of 0.5Ω the minimum inductance was found to be $20\mu H$.

$$L_{MIN} = \frac{(1-D)R}{2f} \tag{D.2}$$

The final step is to establish the required capacitance for smoothing the output. This is determined using the equation below, where $\frac{\Delta V_{OUT}}{V_{OUT}}$ is the output voltage ripple, selected to be 2% (0.02) for this application.

$$C = \frac{1-D}{8L\left(\frac{\Delta V_{OUT}}{V_{OUT}}\right)} \tag{D.3}$$

This resulted in a minimum capacitance value of 1.694nF (increasing the capacitance will reduce the voltage ripple.

D.2 Results

Unfortunately, it was determined that the buck converter was unsuitable for use in the transmitter circuit. The primary cause for this was the load dependence of the buck converter. The circuit was designed to operate with a 0.5Ω load, to be able to provide the required 100 watts of output power. This produced results similar to those in Figure D.2, which was produced in Multisim to aid in testing and troubleshooting of the breadboarded buck converter circuit. In this simulation, the input voltage (V5) was set at 20 volts, and the output voltage (V3) rippled around 6 to 7 volts. Unfortunately, with the $1k\Omega$ load used for low power testing, instead of producing the expected voltage reduction, output a voltage rippling around the full input voltage. It was determined that the lack of current through the inductor at small loads was the cause of this problem. This is unacceptable, since it is anticipated that the load will vary based on the current needs of the battery charging circuit attached to the receiver.

Figure D.2: Simulation of buck converter with $20V$ supply and 0.5Ω load (Consistent with results from breadboarded circuit)

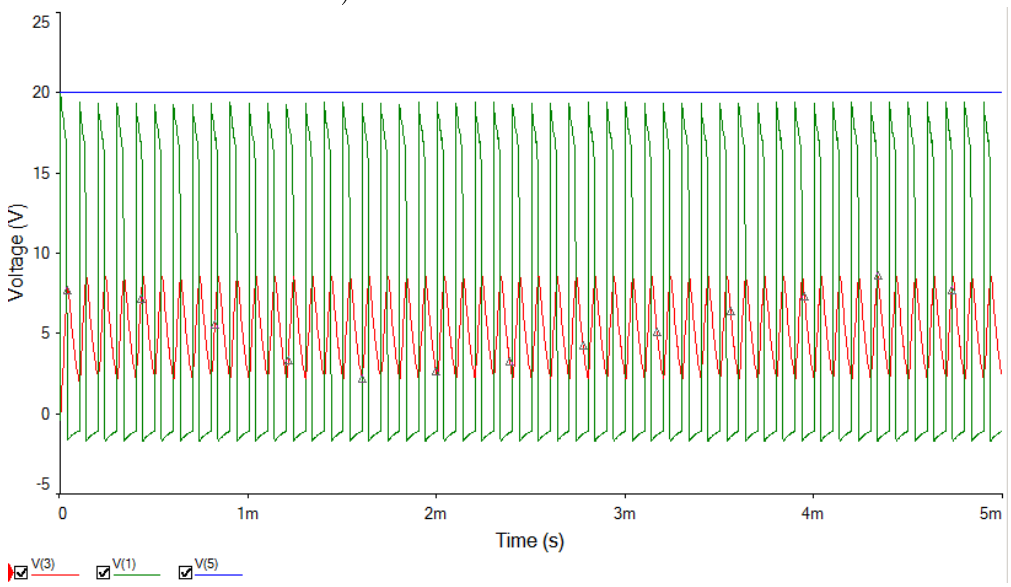

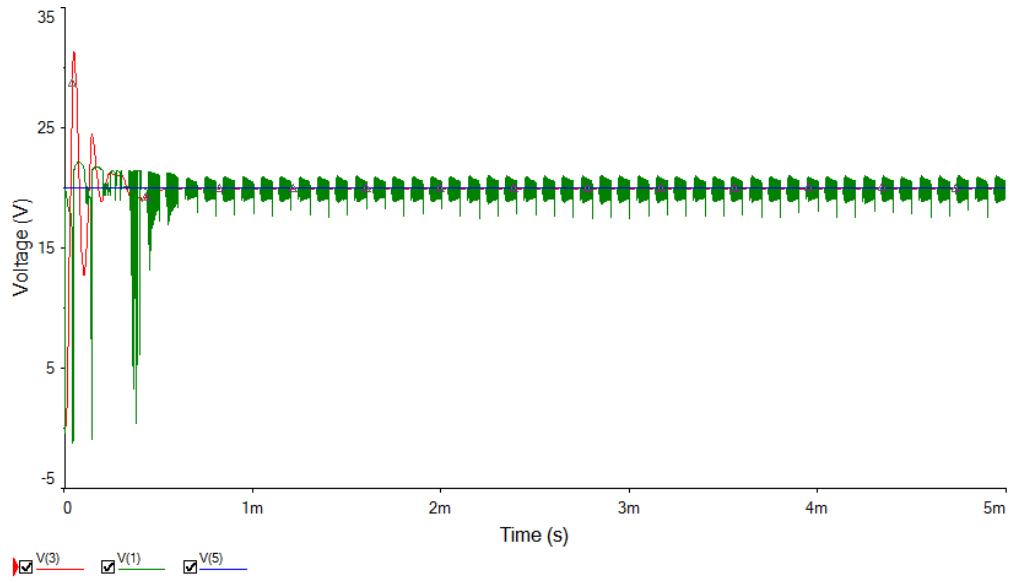

Figure D.3: Simulation of buck converter with $20V$ supply and $1k\Omega$ load (Consistent with results from breadboarded circuit)